Stellar, brown dwarf and multiple star properties from hydrodynamical simulations of star cluster formation

Matthew R. Bate[⋆]

School of Physics, University of Exeter, Stocker Road, Exeter EX4 4QL

ABSTRACT

We report the statistical properties of stars, brown dwarfs and multiple systems obtained from the largest hydrodynamical simulation of star cluster formation to date that resolves masses down to the opacity limit for fragmentation (a few Jupiter masses). The simulation is essentially identical to that of Bate, Bonnell & Bromm except that the initial molecular cloud is larger and more massive. It produces more than 1250 stars and brown dwarfs, providing unprecedented statistical information that can be compared with observational surveys. The calculation uses sink particles to model the stars and brown dwarfs. Part of the calculation is rerun with smaller sink particle accretion radii and gravitational softening to investigate the effect of these approximations on the results.

We find that hydrodynamical/sink particle simulations can reproduce many of the observed stellar properties very well. Multiplicity as a function of the primary mass, the frequency of very low mass (VLM) binaries, general trends for the separation and mass ratio distributions of binaries and the relative orbital orientations of triples systems are all in reasonable agreement with observations. We also examine the radial variations of binarity, velocity dispersion and mass function in the resulting stellar cluster and the distributions of disc truncation radii due to dynamical interactions. For VLM binaries, because their separations are typically close, we find that their frequency is sensitive to the sink particle accretion radii and gravitational softening used in the calculations. Using small accretion radii and gravitational softening results in a frequency of VLM binaries similar to that expected from observational surveys ($\approx$20 per cent). We also find that VLM binaries evolve from wide, unequal-mass systems towards close equal-mass systems as they form. The two main deficiencies of the calculations are that they overproduce brown dwarfs relative to stars and that there are too few unequal-mass binaries with K- and G-dwarf primaries. The former of these is likely due to the absence of radiative feedback and/or magnetic fields.

Key words: binaries: general – stars: formation – stars: kinematics – stars: low-mass, brown dwarfs – stars: luminosity function, mass function – ISM: clouds.

1 INTRODUCTION

Understanding the origin of the statistical properties of stellar systems is the fundamental goal of a complete theory of star formation. In terms of their impact on galaxy formation and evolution, the most important statistical properties are probably the stellar initial mass function (IMF) and the star formation rate and efficiency. However, for understanding the formation and evolution of stellar clusters, stellar systems themselves, protoplanetary discs and planetary systems, many more statistical properties are important. Furthermore, there are currently many models that have been proposed for the

origin of the IMF (see the recent review of Bonnell, Larson & Zinnecker 2007 or the introduction of Bate & Bonnell 2005, hereafter BB2005). Many of these are able to explain qualitatively the observed form of the IMF, but most of these do not predict other statistical properties. A complete model must be able to explain the origin of all the statistical properties of stellar systems, and how these depend on variations in environment and initial conditions. Along with the IMF and star formation rate and efficiency, these other statistical properties include the structure of stellar clusters and stellar velocity dispersions, the properties of multiple stellar systems, jets, protoplanetary discs, and the rotation rates and magnetic fields of stars. In particular, when considering binary, triple and higher-order multiple stellar systems, there are many statistical properties that require understanding such as their frequencies, their

[⋆]E-mail: mbate@astro.ex.ac.uk

mass ratios, their orbital separations and eccentricities, relations between orbits and mass ratios in hierarchical systems, and relative stellar rotations.

To investigate the origin of a wide range of statistical properties of stars directly through hydrodynamical calculations is difficult because it is necessary to produce a large number of objects (to get statistically significant results) and to use high resolution (to model low-mass objects such as brown dwarfs, multiple systems and circumstellar discs). One approach is to perform a large number of high-resolution calculations of the collapse of isolated small molecular cloud cores (e.g. Delgado-Donate, Clarke & Bate 2004; Delgado-Donate et al. 2004; Goodwin, Whitworth & Ward-Thompson 2004a,b,c, 2006). Such calculations have been able to qualitatively match some of the observed statistical properties of stellar systems. For example, Delgado-Donate et al. (2004) found that multiplicity is an increasing function of primary mass (though they obtained a steeper function than is observed). Goodwin et al. (2004c) found that star formation in small cores might be a good explanation for the somewhat unusual stellar mass function in Taurus (namely the relatively high proportion of stars with masses $\approx 1 \, M_\odot$). However, such calculations are not applicable to denser star-forming regions since they neglect interactions between cores and protostellar systems. Furthermore, they use an arbitrary population of dense cores for their initial conditions, which may or may not be a good representation of real dense cores.

Over the past few years, we have performed large-scale hydrodynamical calculations of the collapse and fragmentation of turbulent molecular clouds to investigate the origins of stellar properties (Bate, Bonnell & Bromm 2002a,b, 2003, hereafter BBB2003; BB2005; Bate 2005, hereafter B2005). In these large-scale calculations, dense cores are formed self-consistently from hydrodynamical flows on larger scales, and interactions between dense cores and protostellar systems occur naturally. These calculations have differed from most other large-scale hydrodynamical star formation calculations in that they modelled clouds that were large enough to produce dozens of stars and yet *simultaneously* they resolved down to and beyond the opacity limit for fragmentation. Thus, they resolved the entire mass function, capturing the formation of all stars and brown dwarfs. They also allowed discs with sizes down to ≈ 10 au and binaries with separations of a few astronomical units to be resolved. Earlier similar large-scale hydrodynamical calculations (Klessen, Burkert & Bate 1998; Klessen & Burkert 2000; Bonnell et al. 2001; Klessen 2001; Klessen & Burkert 2001; Bonnell & Bate 2002; Bonnell, Bate & Vine 2003) formed large numbers of stars, but were unable to resolve brown dwarfs, most binaries and discs. All these calculations used smoothed particle hydrodynamics (SPH) with sink particles to model the star-forming clouds. Most recently, grid-based adaptive mesh refinement (AMR) calculations have also begun to compete, forming up to a few dozen objects and resolving discs and binaries (Li et al. 2004; Offner, Klein & McKee 2008). However, regardless of whether SPH or AMR has been used, even the largest high-resolution large-scale calculations published to date have only formed a few dozen stars and brown dwarfs, making it difficult to compare the results with observations in any detail.

In this paper, we report the results from two large-scale hydrodynamical calculations of the collapse and fragmentation of turbulent molecular clouds. The calculations follow the evolution of $500 \, M_\odot$ clouds (similar to the calculation presented by BBB2003, but an order of magnitude more massive) to form hundreds of stars and brown dwarfs. Two versions of the same calculation are performed, one with sink particles with radii of 5 au (as in BBB2003) and a

rerun version that has sink particle radii of only 0.5 au, but which is not followed as far. The large accretion radii calculation forms 1254 stars and brown dwarfs in 1.5 initial cloud free-fall times. This large number of objects allows us, for the first time, to make a meaningful comparison of the statistical properties of stars and binary and multiple systems with observations.

This paper is structured as follows. In Section 2, we briefly describe the numerical method and the initial conditions for the simulations. In Section 3, we present our results and compare them with the results of observational surveys. Our conclusions are given in Section 4.

2 COMPUTATIONAL METHOD

The calculations presented here were performed using a three-dimensional SPH code. The SPH code is based on a version originally developed by Benz (Benz 1990; Benz et al. 1990). The smoothing lengths of the particles are variable in time and space, subject to the constraint that the number of neighbours for each particle must remain approximately constant at $N_{\text{neigh}} = 50$. The SPH equations are integrated using a second-order leapfrog integrator with individual time-steps for each particle. Gravitational forces between particles and a particle's nearest neighbours are calculated using a binary tree. We use the standard form of artificial viscosity (Monaghan & Gingold 1983; Monaghan 1992) with strength parameters $\alpha_v = 1$ and $\beta_v = 2$. Further details can be found in Bate, Bonnell & Price (1995). The code has been parallelized by M. Bate using OPENMP.

2.1 Equation of state

To model the thermal behaviour of the gas without performing radiative transfer, we use a barotropic equation of state for the thermal pressure of the gas $p = K \rho^\eta$, where K is a measure of the entropy of the gas. The value of the effective polytropic exponent η varies with density as

$$\eta = \begin{cases} 1, & \rho \leq \rho_{\text{crit}}, \\ 7/5, & \rho > \rho_{\text{crit}}. \end{cases} \tag{1}$$

We take the mean molecular weight of the gas to be $\mu = 2.46$. The value of K is defined such that when the gas is isothermal $K = c_s^2$, with the sound speed $c_s = 1.84 \times 10^4 \, \text{cm s}^{-1}$ at 10 K, and the pressure is continuous when the value of η changes.

The value of the critical density above which the gas becomes non-isothermal is set to $\rho_{\text{crit}} = 10^{-13} \, \text{g cm}^{-3}$. This equation of state has been chosen to match the relationship between temperature and density closely during the spherically symmetric collapse of molecular cloud cores with solar metallicity as calculated with frequency-dependent radiative transfer (e.g. Masunaga & Inutsuka 2000). The equation of state is discussed further by BBB2003.

The heating of the molecular gas that begins at the critical density inhibits fragmentation at higher densities. This effect is known as the opacity limit for fragmentation (Low & Lynden-Bell 1976; Rees 1976; Silk 1977a,b; Boyd & Whitworth 2005). It results in the formation of distinct pressure-supported fragments within collapsing gas because the temperature increases quickly enough with density that the Jeans mass increases, and the high-density region that was collapsing becomes Jeans stable. These regions stop collapsing and can only contract as they accrete mass. The value of the initial mass of a fragment presumably also gives the minimum mass for a brown dwarf, since any subsequent accretion will only increase a

fragment's mass. This minimum mass depends on the value of the critical density and is approximately equal to the Jeans mass at that density and temperature. The lowest mass object produced by the calculations was ≈ 4 Jupiter masses (M_J).

2.2 Sink particles

As the pressure-supported fragments accrete, their central density increases, and it becomes computationally impractical to follow their internal evolution because of the short dynamical time-scales involved. Therefore, when the central density of a pressure-supported fragment exceeds $\rho_s = 1000\rho_{crit}$, we insert a sink particle into the calculation (Bate et al. 1995). This value of ρ_s is a factor of 10 higher than in earlier calculations (e.g. BBB2003), which allows more time for an object to merge or be disrupted before being replaced by a sink particle.

In the main calculation discussed in this paper, a sink particle is formed by replacing the SPH gas particles contained within $r_{acc} = 5$ au of the densest gas particle in a pressure-supported fragment by a point mass with the same mass and momentum. Any gas that later falls within this radius is accreted by the point mass if it is bound, and its specific angular momentum is less than that required to form a circular orbit at radius r_{acc} from the sink particle. Thus, gaseous discs around sink particles can only be resolved if they have radii $\gtrsim 10$ au. Sink particles interact with the gas only via gravity and accretion. The angular momentum accreted by a sink particle is recorded but plays no further role in the calculation.

Since all sink particles are created from pressure-supported fragments, their initial masses are several M_J, as given by the opacity limit for fragmentation. Subsequently, they may accrete large amounts of material to become higher-mass brown dwarfs ($\lesssim 75 M_J$) or stars ($\gtrsim 75 M_J$), but *all* the stars and brown dwarfs begin as these low-mass pressure-supported fragments.

In the main calculation, the gravitational acceleration between two sink particles is Newtonian for $r \geq 4$ au, but is softened within this radius using spline softening (Benz 1990). The maximum acceleration occurs at a distance of ≈ 1 au; therefore, this is the minimum separation that a binary can have even if, in reality, the binary's orbit would have been hardened.

Part of the main calculation was rerun from just before the first star formed with sink particle accretion radii of $r_{acc} = 0.5$ au and with *no gravitational softening between sink particles*. This was done to investigate the dependence of the results on these approximations. This partial rerun (henceforth referred to as the rerun calculation) could not be followed as long as the main calculation due to the smaller time-steps required.

Sink particles were permitted to merge in either calculation if they passed within 0.02 au of each other (i.e. $\approx 4 \, R_{\odot}$). This radius was chosen because recently formed protostars are thought to have relatively large radii (e.g. Larson 1969). Again, this differs from previous similar calculations. In the main calculation, 23 mergers occurred and in the rerun calculation, 20 mergers occurred (in a shorter period of time).

The benefits and potential problems associated with introducing sink particles are discussed in more detail in BBB2003 and will be further examined in this paper.

2.2.1 Identification of multiple stellar systems

With the calculations presented in this paper producing many hundreds of stars and brown dwarfs, it is important to automate the

analysis as much as possible. Much of this is straightforward. However, in order to analyse binaries and multiple stellar systems, we first need to identify them. This is done as follows.

At the end of each calculation, we essentially construct a structure 'tree'. We begin with every star or brown dwarf (sink particle) being a 'node'. We then loop over all pairs of nodes calculating the closest pair of 'nodes' that are gravitationally bound to each other (i.e. the sum of their relative gravitational and kinetic energies is negative). This pair of 'nodes' then becomes a new node and the original nodes are removed. For example if the two nodes are single stars then these nodes are replaced by a new node containing a binary that is located at the binary's centre of mass and has the binary's mass and centre-of-mass velocity. If one node is a binary and the other is a single star, the new node contains a triple system. This process is then repeated until no new nodes are formed. The result is a structure tree that contains single objects (e.g. some that might have been ejected), binaries or multiples that are not bound to any other node, and some nodes which may contain clusters of dozens or hundreds of stars and brown dwarfs, many of which may also be binaries or multiples within these clusters.

The observant reader may note later in the paper that there are a few binaries that have separations of several thousand astronomical units. These have been checked manually. They are wide binaries in the periphery of the cluster. They are composed of ejected objects that happen to be gravitationally bound to one another due to their similar ejection velocities.

2.3 Initial conditions

The initial conditions are essentially identical to the calculation of Bate et al. (2002a,b) and BBB2003, except that the cloud has 10 times the mass and a larger radius so as to give the same initial density, and a larger Mach number so as to balance the turbulent and gravitational energies initially. A 500 $M_{\odot}$ molecular cloud was set up as a uniform density sphere. The cloud's radius was set to 0.404 pc (83 300 au). At the initial temperature of 10 K, the mean thermal Jeans mass is 1 $M_{\odot}$ (i.e. the cloud contains 500 thermal Jeans masses).

Although the cloud was uniform in density, we imposed an initial supersonic 'turbulent' velocity field in the same manner as Ostriker, Stone & Gammie (2001) and BBB2003. We generated a divergence-free random Gaussian velocity field with a power spectrum $P(k) \propto k^{-4}$, where k is the wavenumber. In three dimensions, this results in a velocity dispersion that varies with distance, λ, as $\sigma(\lambda) \propto \lambda^{1/2}$, in agreement with the observed Larson scaling relations for molecular clouds (Larson 1981). The velocity field was generated on a 128^3 uniform grid and the velocities of the particles were interpolated from the grid. As in BBB2003, the velocity field is normalized so that the kinetic energy of the turbulence equals the magnitude of the gravitational potential energy of the cloud. Thus, the initial rms Mach number of the turbulence was $\mathcal{M} = 13.7$. This is higher than that in BBB2003 (which was $\mathcal{M} = 6.4$).

The initial free-fall time of the cloud was $t_{ff} = 6.0 \times 10^{12}$ s or 1.90×10^5 yr (the same as in BBB2003).

2.4 Resolution

The local Jeans mass must be resolved throughout the calculations to model fragmentation correctly (Bate & Burkert 1997; Truelove et al. 1997; Whitworth 1998; Boss et al. 2000; Hubber, Goodwin & Whitworth 2006). This requires $\gtrsim 1.5 \, N_{neigh}$ SPH particles per Jeans mass; N_{neigh} is insufficient (BBB2003). The minimum Jeans mass

occurs at the maximum density during the isothermal phase of the collapse, $\rho_{crit} = 10^{-13}$ g cm^{-3}, and is ≈ 0.0011 M$_\odot$ (1.1 M_J). Thus, we used 3.5×10^7 particles to model the 500-M$_\odot$ cloud.

The main calculation required approximately 100 000 CPU hours on a 1.65 GHz IBM p570 compute node of the United Kingdom Astrophysical Fluids Facility (UKAFF), while the rerun calculation took approximately half as long.

3 RESULTS

The main calculation is the largest simulation of star cluster formation to date in which collapsing gas is resolved down to the opacity limit for fragmentation. The simulation is similar to that presented by BBB2003, but is of a more massive cloud. The main purpose of performing the simulation was simply to provide much more accurate statistical information. BBB2003 only formed 50 stars and brown dwarfs, whereas the main calculation here forms 1254 stars and brown dwarfs in $1.50t_{ff}$ (285 350 yr), and even the rerun calculation that uses smaller accretion radii and no gravitational softening produces 258 objects in $1.038t_{ff}$ (197 460 yr). See Table 1 for a summary of the statistics, including the numbers of stars and brown dwarfs produced by the end of the two calculations, the total mass that has been converted to stars and brown dwarfs and the mean stellar mass.

In BBB2003, although binaries and higher-order multiple systems were produced by the simulation, with such small numbers of objects little could be said about their statistical properties. Even adding together the results of the three simulations presented by BBB2003, BB2005 and B2005 (which had different initial conditions or thermal physics), provides 22 binary systems, 15 of which are components of triple and/or quadruple systems. By contrast, the new calculations presented here provide a wealth of binary and high-order multiple systems. The main calculation produced 90 binary, 23 triple and 25 quadruple systems, including 38 very low mass (VLM) multiples in which all components are VLM (masses less than 0.1 M$_\odot$). Note that throughout the rest of this paper we will usually refer to VLM objects rather than brown dwarfs in order to allow better comparison to be made with the observational surveys that often combine studies of VLM stars and high-mass brown dwarfs in order to increase the sample sizes. At times, we will also make a distinction between VLM objects and low-mass brown dwarfs. The latter are the subset of VLM objects whose masses are less than 0.03 M$_\odot$ (30 Jupiter masses). The rerun calculation produced 17 binary, six triple and 17 quadruple systems including 13 VLM multiples. Thus, we have the ability not just to examine the frequencies of binary stars and VLM objects, but

binarity as a function of primary mass, and the separation and mass ratio distributions.

The star formation process itself is similar to that seen in BBB2003, BB2005 and B2005. Fig. 1 shows snapshots of column density from the main calculation illustrating the global evolution. The initial turbulent velocity field generates structures with those that are strongly self-gravitating collapsing to form stellar groups and clusters. The main difference from the earlier calculations is that with such a large cloud at least five subclusters containing dozens to hundreds of objects form ($t \approx 1.10$–$1.20t_{ff}$), and then merge together to form a single dense stellar cluster by the end of the calculation. Such hierarchical buildup of a stellar cluster was previously highlighted in the lower resolution simulation of a 1000 M$_\odot$ cloud performed by Bonnell et al. (2003). The evolution of the cloud and the formation and merger of the subclusters are best viewed in an animation. Animations of the main calculation can be downloaded from http://www.astro.ex.ac.uk/people/mbate/Cluster/ both in the colour scheme of Fig. 1 and as a three-dimensional red-cyan movie. Unfortunately, the resolved circumstellar discs and binary systems are not visible on the scale of Fig. 1; however, with well over 100 multiple systems, it is impossible to display these in a paper. In Fig. 2, we display the global evolution of the rerun calculation. There are no substantial differences on large scales between the two calculations, with the exception of the different pattern of ejected objects visible at $t = 1.00t_{ff}$ (cf. the two panels in Figs 1 and 2). Since the dynamics of individual stellar systems are chaotic, even changing the sink particle parameters on very small scales affects the outcomes of dynamical interactions. In the following sections of the paper, we examine the statistical properties of the stellar systems.

3.1 The initial mass function

The IMF produced by the end of the main calculation is shown in Fig. 3 and is compared with the parametrizations of the observed IMF given by Chabrier (2003), Kroupa (2001) and Salpeter (1955). The IMFs obtained from BBB2003 and B2005 were, within the statistical uncertainties, consistent with the observed IMF. However, the IMF from the main calculation reported here is much more accurately determined and is clearly not consistent with the observed IMF. The computed IMF has a similar overall form to the observed IMF, with a reasonable Salpeter-type slope at the high-mass end, a flattening below a solar mass and an eventual turnover. However, it significantly overproduces brown dwarfs. The calculation produces 459 stars and 795 brown dwarfs (masses <0.075 M$_\odot$). Even taking into account that 46 of the brown dwarfs are still accreting when

Table 1. The parameters and overall statistical results for the BBB2003 calculation and the two calculations presented here. The initial conditions were similar except that the two calculations presented here are of more massive, larger clouds than that presented by BBB2003. In particular, the initial densities and mean thermal Jeans masses were identical. In each case, the magnitudes of the initial turbulent velocity fields were scaled so that the kinetic energy equalled the magnitude of the gravitational potential energy. The calculations were run for different numbers of initial cloud free-fall times. Brown dwarfs are defined as having final masses less than 0.075 M$_\odot$. The numbers of stars (brown dwarfs) are lower (upper) limits because some of the brown dwarfs were still accreting when the calculations were stopped. The only difference between the main and rerun calculations presented here are in the accretion radii and gravitational softening of the sink particles, and the fact that the evolution of the rerun calculation could not be followed as long due to computational limitations.

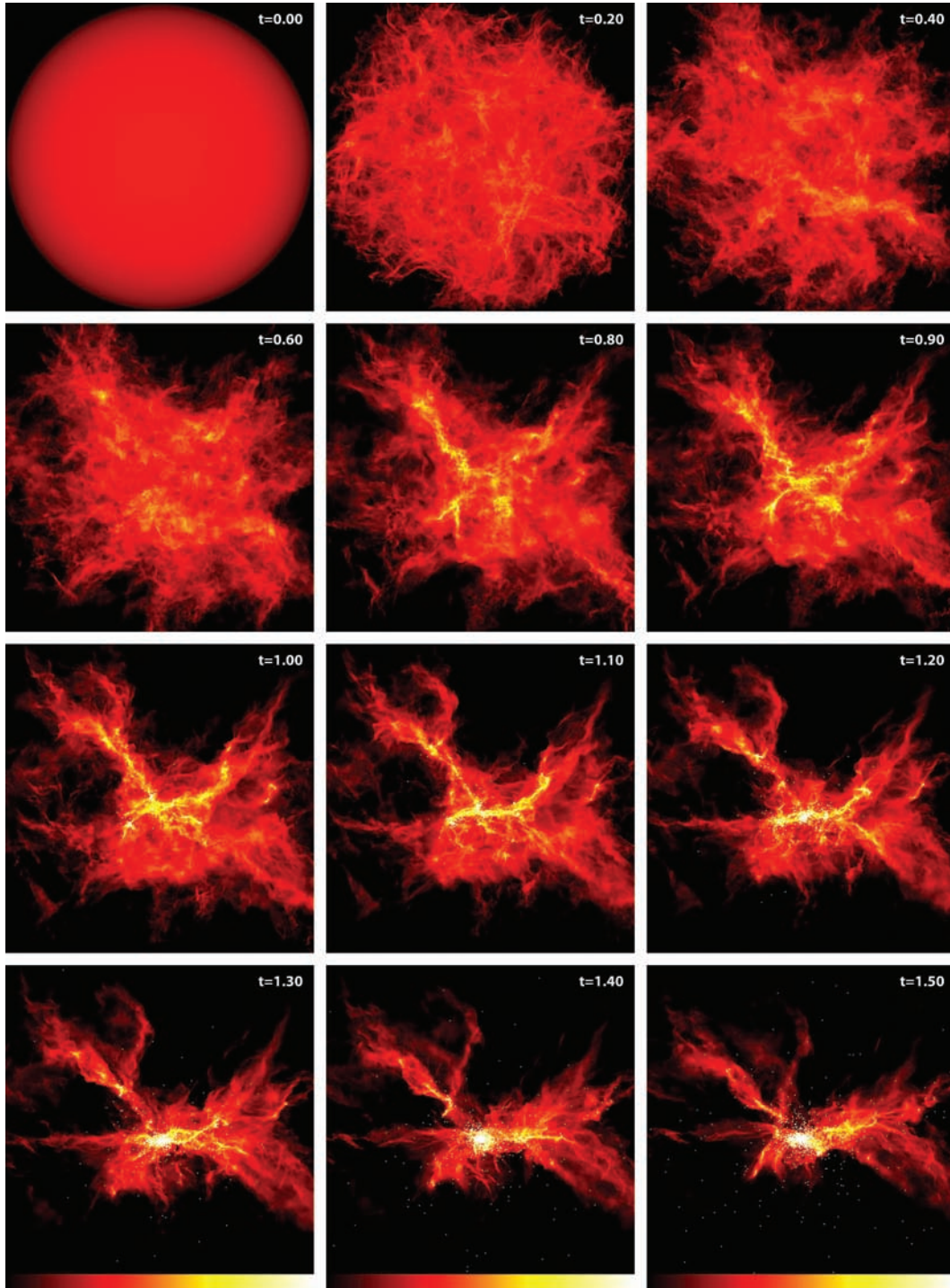| Calculation	Initial gas mass M$_\odot$	Initial radius pc	Jeans mass M$_\odot$	Mach number	Accretion radii au	Gravity softening au	End time t_{ff}	No. stars formed	No. brown dwarfs formed	Mass of stars & brown dwarfs M$_\odot$	Mean Mass M$_\odot$
BBB2003	50	0.188	1	6.4	5	4	1.40	≥ 23	≤ 27	5.9	0.12
Main	500	0.404	1	13.7	5	4	1.50	≥ 459	≤ 795	191	0.15
							1.04	≥ 102	≤ 119	32.6	0.15
Rerun	500	0.404	1	13.7	0.5	0	1.04	≥ 94	≤ 164	32.0	0.12

Figure 1. The global evolution of the main calculation. Shocks lead to the dissipation of the turbulent energy that initially supports the cloud, allowing parts of the cloud to collapse. Star formation begins at $t = 0.715t_{\rm ff}$ in a collapsing dense core. By $t = 1.20t_{\rm ff}$, the cloud has produced five main subclusters, and by the end of the calculation four out of five of these subclusters have merged into a single large cluster. Each panel is 0.8 pc (165 000 au) across. Time is given in units of the initial free-fall time, $t_{\rm ff} = 1.90 \times 10^5$ yr. The panels show the logarithm of column density, N, through the cloud, with the scale covering $-1.4 < \log N < 1.0$ with N measured in g cm^{-2}.

the calculation is stopped and may eventually reach stellar masses, the ratio of brown dwarfs to stars is at least 3:2, whereas recent observations suggest that the IMF produces more stars than brown dwarfs (Greissl et al. 2007; Luhman 2007; Andersen et al. 2008). Andersen et al. (2008) find that the ratio of stars with masses 0.08–

$1.0\,{\rm M_\odot}$ to brown dwarfs with masses 0.03–$0.08\,{\rm M_\odot}$ is $N(0.08$–$1.0)/N(0.03$–$0.08) \approx 5 \pm 2$. For the main calculation, this ratio is $408/326 = 1.25$. Although the IMF below $0.03\,{\rm M_\odot}$ is not yet well constrained observationally, the number of objects seems to be decreasing for lower masses. Thus, it is unlikely that the true ratio of
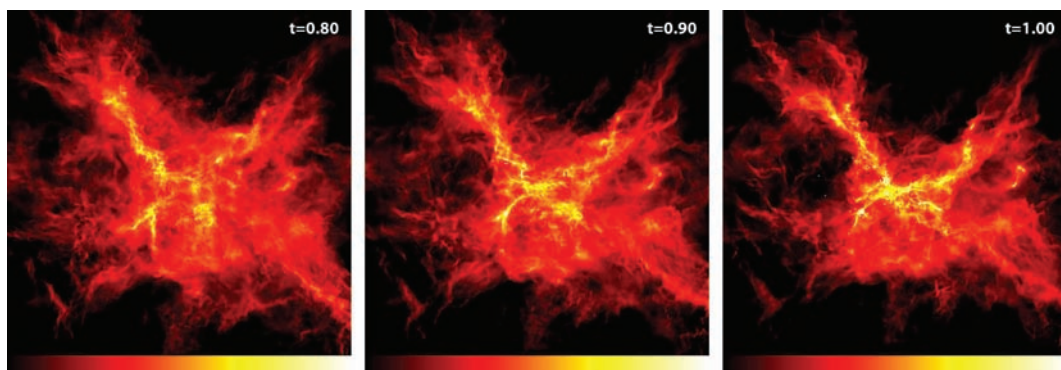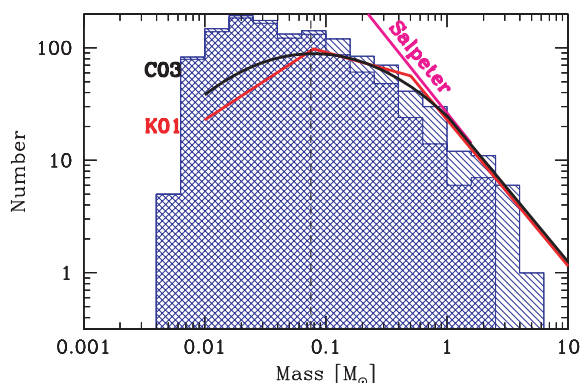
Figure 2. The global evolution of the rerun calculation with smaller sink particle accretion radii and no gravitational softening between sink particles. The global evolution is very similar to the main calculation, but due to the chaotic nature of the dynamics on small scales, the detailed structure of the multiple systems and the ejections differs. The calculation is only followed to just over one free-fall time because it is much more computationally expensive. Each panel is 0.8 pc (165 000 au) across. Time is given in units of the initial free-fall time, $t_{ff} = 1.90 \times 10^5$ yr. The panels show the logarithm of column density, N, through the cloud, with the scale covering $-1.4 < \log N < 1.0$ with N measured in g cm^{-2}.

Figure 3. Histograms giving the IMF of the 1254 stars and brown dwarfs that had been produced by the end of the main calculation. The single-hashed region gives all objects, while the double-hashed region gives those objects that have stopped accreting. Parametrizations of the observed IMF by Salpeter (1955), Kroupa (2001) and Chabrier (2003) are given by the magenta line, red broken power law and black curve, respectively. The numerical IMF broadly follows the form of the observed IMF, with a Salpeter-like slope above $\sim 0.5\,M_\odot$ and a turnover at low masses. However, it clearly overproduces brown dwarfs by a factor of ≈ 4.

brown dwarfs to stars exceeds 1:3. The main calculation, therefore, overproduces brown dwarfs relative to the stars by a factor of ≈ 4 compared with the observed IMF.

3.1.1 The dependence of the IMF on numerical approximations and missing physics

There are several potential causes of brown dwarf overproduction that may be divided into two categories: numerical effects or neglected physical processes. Arguably, the main numerical approximation made in the calculations is that of the sink particles. High-density gas is replaced by a sink particle whenever the maximum density exceeds 10^{-10} g cm^{-3}, and the gas within a radius of 5 au is accreted on to the sink particle producing a gravitating point mass containing a few Jupiter masses of material. These sink particles then interact with each other ballistically, which, for example, might plausibly artificially enhance ejections and the production of low-mass objects.

In order to investigate the effect of the sink particle approximation on the results, we reran part of the main calculation with smaller sink particles (accretion radii of 0.5 au) and without gravitational softening between sink particles (they were allowed to merge if they came within $4\,R_\odot$ of each other.) This calculation was only followed to $1.038t_{ff}$ due to its much more time consuming nature. The small accretion radius calculation produced 258 stars and brown dwarfs in the same time-period that the main calculation produced 221 objects. Because the calculations are chaotic, identical results should not be expected. The main question to answer is whether or not the results are statistically different.

In Figs 4 and 5, we compare the IMFs produced by the main calculation and the smaller sink particle calculation at the same time. The smaller sink particle calculation produces twice as many objects with masses less than 10 Jupiter masses than the main calculation, but overall the two IMFs are very similar. A Kolmogorov–Smirnov (K–S) test run on the two distributions shows that they have a 13 per cent probability of being drawn from the same underlying IMF (i.e. they are statistically indistinguishable). Removing objects with less than 10 Jupiter masses from the K–S test results in a 38 per cent probability of the two distributions being drawn from the same underlying IMF. We conclude that the variations in the sink particle accretion radii and gravitational softening may have an effect on the production of extremely low mass objects. However, changes in the sink particle parameters do not significantly alter the overall results and, thus, the use of sink particles is probably not responsible for the significant overproduction of brown dwarfs.

It seems most likely that the overproduction of brown dwarfs is related to the physical processes that are not included in the calculations. Whitehouse & Bate (2006) showed that replacing the barotropic equation of state by radiative transfer can lead to temperatures up to an order of magnitude higher near young low-mass protostars and, thus, potentially strongly inhibits fragmentation. Krumholz (2006) made a similar argument analytically. Furthermore, in purely hydrodynamical/sink particles star cluster formation calculations, many of the brown dwarfs formed originate via disc fragmentation (e.g. Bate et al. 2002a found that 3/4 of the brown dwarfs originated from disc fragmentation). Rafikov (2005), Matzner & Levin (2005), Kratter & Matzner (2006) and Whitworth & Stamatellos (2006) have all pointed out that accurate treatments of radiative transfer are likely to significantly decrease disc fragmentation. Along with the likely effect of radiative feedback on
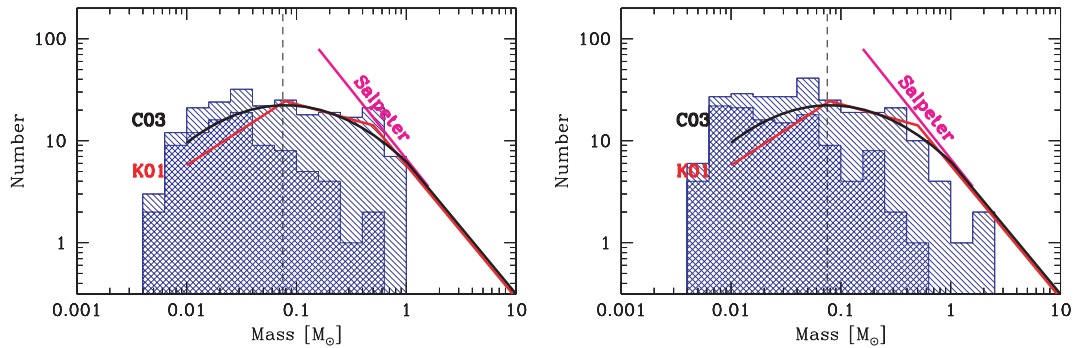
Figure 4. Histograms giving the IMF of the 221 stars and brown dwarfs at $t = 1.038t_{ff}$ in the main calculation (left-hand panel), and the 258 objects formed at the same time in the rerun calculation with smaller sink particle accretion radii and no gravitational softening between sink particles (right-hand panel). The rerun calculation appears to produce a few more very low-mass brown dwarfs (masses less than 10 Jupiter masses), but even this difference is not statistically significant (see Fig. 5), so we conclude that changing the sink particle parameters does not adversely affect the resulting IMF. Comparing the left-hand panel with the IMF in Fig. 3 at the end of the main calculation, we find that much of the overproduction of brown dwarfs occurs late in the calculation (see also Fig. 6).
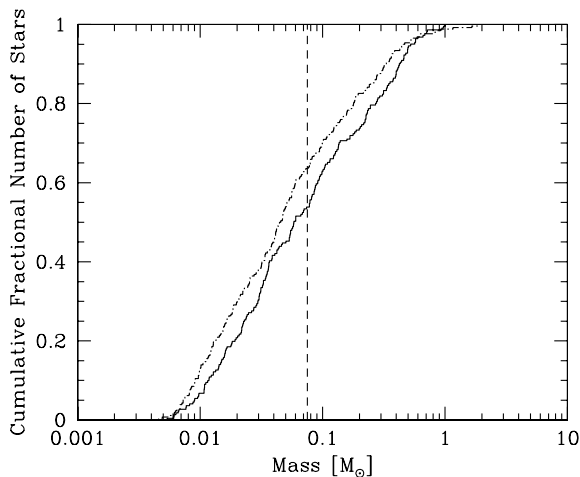

Figure 5. The cumulative IMFs from the main calculation (solid line) and the rerun calculation with small accretion radii (dot–dashed line) both at 1.038 t_{ff} (see Fig. 4 for differential graphs of the IMFs). The calculation with the smaller accretion radii seems to produce more very low-mass brown dwarfs with masses less than 10 Jupiter masses. However, even with this apparent difference, a K–S test on the two distributions gives a 13 per cent probability that the two IMFs were drawn from the same underlying distribution (i.e. they are statistically indistinguishable). Thus, the results do not seem to be adversely affected by the sink particle approximation.
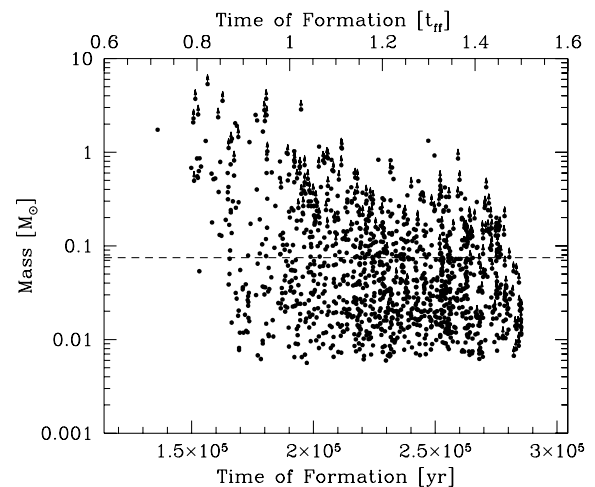

Figure 6. Time of formation and mass of each star and brown dwarf at the end of the main calculation. It is clear that the objects that are the most massive at the end of the calculation are actually some of the first to collapse and form sink particles. Furthermore, the longer the calculation proceeds, the higher the ratio brown dwarfs to stars becomes. Objects that are still accreting significantly at the end of the calculation are represented with vertical arrows. The horizontal dashed line marks the star/brown dwarf boundary. Time is measured from the beginning of the calculation in terms of the free-fall time of the initial cloud (top panel) or years (bottom panel).

fragmentation, we note that as the main calculation progresses, the ratio of low- to high-mass objects increases. This can be seen in Fig. 6 which plots the final mass of an object versus its time of formation, as well as by comparing Fig. 3 with the left-hand panel of Fig. 4 which show the IMFs from the main calculations at $t = 1.50$ and $1.038t_{ff}$, respectively. Radiative feedback is likely to heat the entire central cluster region later in the calculation, potentially curtailing the formation of many of the late low-mass objects.

Another possibility is the effect of magnetic fields. Recently, Price & Bate (2007) showed that stronger magnetic fields generally inhibit disc formation and binary formation (see also Hennebelle & Fromang 2008; Hennebelle & Teyssier 2008). Price & Bate (2008) ran star cluster formation simulations similar to BBB2003, but with magnetic fields. They found that the extra pressure support provided by magnetic fields generally decreased the rate of star formation and

the importance of dynamical interactions between objects. Stronger magnetic fields resulted in a decrease in the ratio of brown dwarfs to stars (though the total numbers of objects formed in the calculations were small, ranging from 15 to 69.).

In summary, we have shown for the first time that purely hydrodynamical simulations of star cluster formation over-produce brown dwarfs. This result is statistically robust. This disagreement with observations is most likely due to the negligence of the physical processes of radiative feedback and/or magnetic fields.

3.1.2 The origin of the initial mass function

BB2005 analysed the earlier calculation presented by BBB2003 and another calculation beginning with a denser cloud to determine the origin of the IMF in those calculations (see also B2005). They

found that the IMF resulted from competition between accretion and ejection. There was no significant dependence of the mean accretion rate of an object on its final mass. Rather, there was a roughly linear correlation between an object's final mass and the time between its formation and the termination of its accretion. Furthermore, the accretion on to an object was usually terminated by a dynamical interaction between the object and another system, ejecting the object. Thus, objects formed with VLMs (a few Jupiter masses) and accreted to higher masses until their accretion was terminated, usually, by a dynamical encounter. This combination of competitive accretion and stochastic ejections produced the mass function.

In Figs 7–9, we plot similar figures to those found in BB2005 and B2005. These figures display the same trends as found by BB2005, but with a much greater statistical significance. Fig. 7 gives the time-averaged accretion rates of all the objects formed in the main calculation versus the object's final mass. The time-averaged accretion rate is the object's final mass divided by the time between its formation (i.e. the insertion of a sink particle) and the end of its accretion (defined as the last time its accretion rate drops below $10^{-7}\,M_\odot\,\mathrm{yr}^{-1}$) or the end of the calculation. As in BB2005, there is no dependence of the time-averaged accretion rate on an object's final mass, except that objects need to accrete at a rate at least as quickly as their final mass divided by their age (i.e. the lower right-hand portion of Fig. 7 cannot have any objects lying in it). This means that the most massive stars have higher time-averaged accretion rates than the bulk of the stars and VLM objects. On the other hand, if the calculation were continued longer, objects that are accreting with lower time-averaged accretion rates could also reach high masses.

The mean of the accretion rates is $1.02 \times 10^{-5}\,M_\odot\,\mathrm{yr}^{-1}$, which is within a factor of 2 of the mean accretion rates of the three calcu-

Figure 8. The time between the formation of each object and the termination of its accretion or the end of the main calculation versus its final mass. Objects that are still accreting significantly at the end of the calculation are represented with arrows. As in BBB2003, BB2005 and B2005, there is a clear linear correlation between the time an object spends accreting and its final mass. The solid line gives the curve that the objects would lie on if each object accreted at the mean of the time-averaged accretion rates. The accretion times are given in units of the t_{ff} on the left-hand axes and years on the right-hand axes. The vertical dashed line marks the star/brown dwarf boundary.

Figure 9. For each single object that has stopped accreting by the end of the main calculation, we plot the time of the ejection of the object from a multiple system versus the time at which its accretion is terminated. As in the smaller calculations of BBB2003, BB2005 and B2005, these times are correlated showing that the termination of accretion on to an object is usually associated with dynamical ejection of the object. Open circles give those objects where multiple 'ejections' are detected by the ejection detection algorithm and, hence, the ejection time is ambiguous (see the main text). Binaries have been excluded from the plot because it is difficult to determine when a binary has been ejected.
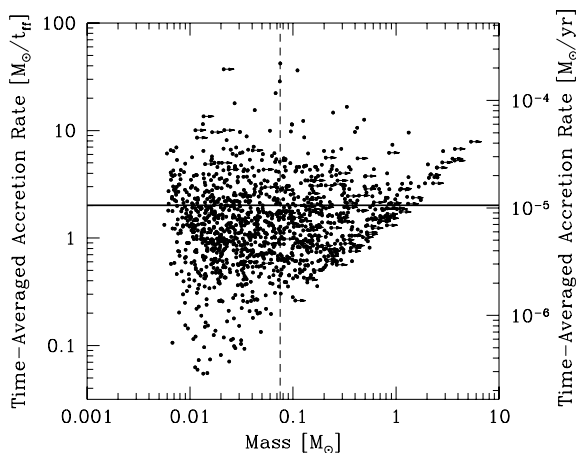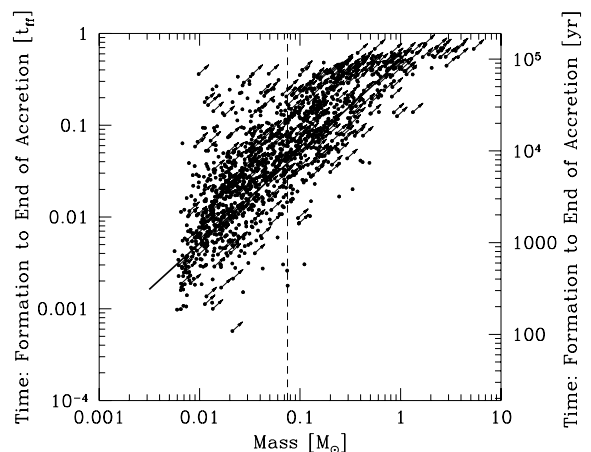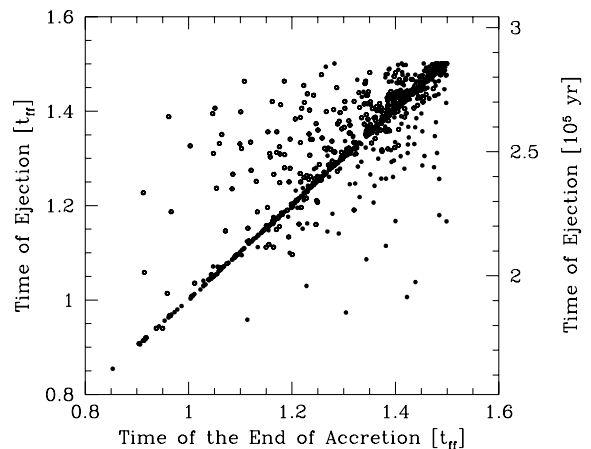

Figure 7. The time-averaged accretion rates of the objects formed in the main calculation versus their final masses. The accretion rates are calculated as the final mass of an object divided by the time between its formation and the termination of its accretion or the end of the calculation. Objects that are still accreting significantly at the end of the calculation are represented with horizontal arrows. There is no dependence of mean accretion rate on final mass for objects with less than $\sim 0.5\,M_\odot$ (and a large dispersion). However, there is a low-accretion rate region of exclusion for the most massive objects since only objects with mean accretion rates greater than their mass divided by their age can reach these high masses during the calculation. The horizontal solid line gives the mean of the accretion rates: $1.02 \times 10^{-5}\,M_\odot\,\mathrm{yr}^{-1}$. The accretion rates are given in $M_\odot/t_{ff}$ on the left-hand axes and $M_\odot\,\mathrm{yr}^{-1}$ on the right-hand axes. The vertical dashed line marks the star/brown dwarf boundary.

lations analysed by BB2005 and B2005. Thus, the mean accretion rate does not depend significantly on cloud density (BB2005), on the equation of state of high-density gas (B2005) or on the total mass of the gas cloud (this work). The dispersion in the accretion rates is about 0.4 dex, also similar to the previous simulations. Rather, the primary determinant of the final mass of a star or brown dwarf is the period over which it accretes. Fig. 8 very clearly shows the

linear relation (with some dispersion) between the period of time over which an object accretes and its final mass.

Finally, in Fig. 9, for each object that has stopped accreting by the end of the main calculation (excluding the components of binaries), we plot the time at which the object undergoes an ejection versus the time that its accretion is terminated. There is a very strong correlation between the two, showing that the accretion is usually terminated by a dynamical encounter with other objects, and confirming the results of BB2005 and B2005. We define the time of ejection of an object as the last time the magnitude of its acceleration drops below 2000 km s^{-1} Myr^{-1} (or the end of the calculation). The acceleration criterion is based on the fact that once an object is ejected from a stellar multiple system, subcluster or cluster through a dynamical encounter, its acceleration will drop to a low value. The specific value of the acceleration was chosen by comparing animations and graphs of acceleration versus time for individual objects. We exclude binaries because they have large accelerations throughout the calculation, which frequently results in false detections of ejections. Also, in Fig. 9, we use two different symbols (filled and open circles). For the former, we are confident of the ejection time. However, for those objects denoted by the open circles, we find that at least two 'ejections' more than 2000 yr apart have occurred. These are usually objects that have had a close dynamical encounter with a multiple system that has put them into long-period orbits rather than ejecting them. In these cases, we chose the 'ejection' time closest to the accretion termination time but we use an open symbol to denote our uncertainty in whether or not we have identified the best time for the dynamical encounter.

In terms of raw results, we find that, excluding binaries, for 635 objects out of 899 (71 per cent), the accretion termination time and the ejection time are within 2000 yr of each other. If we also exclude those objects for which we are uncertain in our identifications of the ejection times as described above, we find 483 objects out of 592 (82 per cent) are consistent with ejection terminating their accretion. These are probably lower limits in the sense that it is difficult to determine in an automated way the time at which an ejection occurs, and an erroneous value is much more likely to differ from the accretion termination time by more than 2000 yr than coincide with it. In any case, it is clear that for the majority of objects, their accretion is terminated by dynamical encounters with other stellar systems.

3.2 Stellar cluster properties

At the end of the main calculation, the bulk of the stars and brown dwarfs are contained within a single compact stellar cluster surrounded by a low-density halo of objects (lower right-hand panel of Fig. 1). The stellar cluster has a half-mass radius of only 10 900 au (0.053 pc), ignoring the gas. The radii containing 80 and 90 per cent of the mass are 29 800 (0.14 pc) and 54 200 au (0.26 pc), respectively.

In Fig. 10, we plot the magnitude of the velocity of every star or brown dwarf relative to the centre of mass of the stellar system at the end of the main calculation. For binaries, we plot the two components with the centre-of-mass velocity of the binary using filled squares connected by a dotted line. The overall rms velocity dispersion (counting each binary only once) is 5.6 km s^{-1} (three dimensional) or 3.2 km s^{-1} (one dimensional). BBB2003, BB2005 and B2005 found no significant dependence of the velocity dispersion on mass. Here, with a much larger sample of objects, we find that stars tend to have a slightly higher dispersion than VLM objects, consistent with observations (e.g.
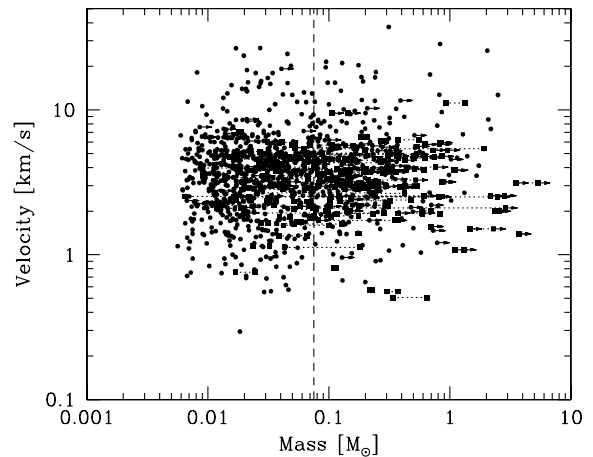

Figure 10. The magnitudes of the velocities of each star and brown dwarf relative to the centre-of-mass velocity of the stellar system at the end of the main calculation. For binaries, the centre-of-mass velocity of the binary is given, and the two stars are connected by dotted lines and plotted as squares rather than circles. Objects still accreting at the end of the calculation are denoted by horizontal arrows. The rms velocity dispersion for the association (counting each binary once) is 5.6 (three dimensional) or 3.2 km s^{-1} (one dimensional). There is a weak dependence of the velocity dispersion on mass with VLM objects having a slightly lower velocity dispersion than stars (see the main text). Binaries are found to have a lower velocity dispersion than single objects of only 3.8 km s^{-1} (three dimensional). The vertical dashed line marks the star/brown dwarf boundary.

Joergens 2006). The rms velocity dispersion of VLM systems is 5.4 km s^{-1} (three dimensional), while for the stars (masses $\geq 0.1\,M_\odot$), the rms velocity dispersion is 6.9 km s^{-1} (three dimensional). Binaries have a velocity dispersion of only 3.8 km s^{-1} (three dimensional), significantly lower than single objects.

Since this is the first hydrodynamical calculation to form a massive stellar cluster while simultaneously resolving brown dwarfs and binaries, it is of interest to examine how the stellar properties vary with radius. We define the cluster centre to be the location of the most massive star ($5.3\,M_\odot$). In Table 2, we present statistics on how the stellar masses, velocity dispersion and binary fraction vary with radius from the cluster centre. Note that for this table, we have defined the binary fraction as the number of binaries divided by the number of systems (single objects and binaries). We do not make any attempt to identify triple or higher-order systems. Each binary is counted once and its centre-of-mass velocity is used when calculating the stellar velocity dispersions.

We find that within the radius containing 80 per cent of the mass (excluding the gas), there is little evidence of a radial variation in the stellar mass function (see Fig. 11), the velocity dispersion or the binary fraction. The exception may be the very centre of the cluster (within 1000 au of the most massive star) where the median stellar mass, the upper quartile mass, the velocity dispersion and the binary fraction are all higher than in the bulk of the cluster. However, there are only eight objects in this region so the statistical uncertainties are great.

In the periphery of the cluster containing 20 per cent of the stellar mass (perhaps better described as the halo), we do find statistically significant differences. The mass function is still indistinguishable from the mass function found in the bulk of the cluster (the median, the upper quartile mass and the maximum mass are all similar to those values found in the bulk of the cluster.). However, the velocity dispersion increases monotonically as the distance from the cluster

Table 2. Radial properties of the stellar cluster at the end of the main calculation. The cluster is very compact with a half-mass radius of 10 900 au. The radii containing 80 and 90 per cent of the mass are 29 800 and 54 200 au, respectively. There is no evidence for radial mass segregation in terms of the median mass, the upper quartile mass and the maximum mass, except in the inner 1000 au. In terms of the binary fraction and the stellar velocity dispersion, again the very centre of the cluster has a higher velocity dispersion and a higher binary frequency than the bulk of the cluster. However, unlike the mass function, the velocity dispersion and binary fraction also differ in the outer regions of the cluster (the outer 20 per cent of the mass, beyond three half-mass radii). The outer regions have a higher velocity dispersion and a lower binary fraction than the bulk of the cluster.

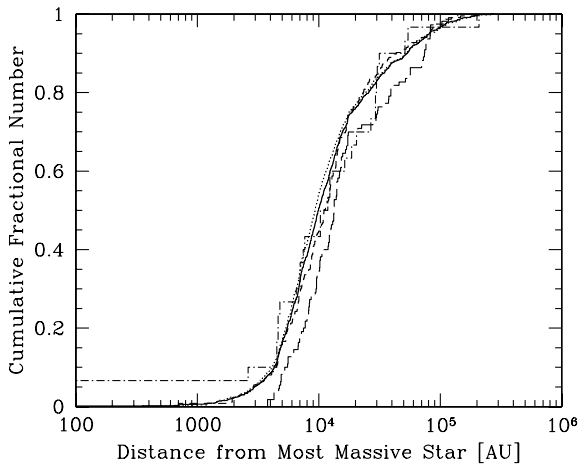| Quantity/distance range	<1000 au	1000–3000 au	3000×10^4 au	$1-3 \times 10^4$ au	$3-10 \times 10^4$ au	$>1 \times 10^5$ au
Median mass [$M_\odot$]	0.18	0.024	0.035	0.056	0.054	0.045
Upper quartile mass [$M_\odot$]	0.30	0.091	0.098	0.15	0.18	0.095
Maximum mass [$M_\odot$]	5.3	2.9	3.7	2.5	2.1	2.0
Velocity dispersion [km s^{-1}]	6.1	4.0	4.2	4.3	8.2	13.8
Number objects	8	56	569	408	172	41
Number binaries	2	8	68	55	13	0
Binary fraction	0.33	0.167	0.136	0.156	0.082	0.0

Figure 11. The cumulative fractions of stars as a function of distance from the most massive star at the end of the main calculation. The solid line gives the result for all stars, while the dotted, short-dashed, long-dashed and dot–dashed lines give the cumulative distributions for the stellar mass ranges $M < 0.1, 0.1 \leq M < 0.3, 0.3 \leq M < 1.0$ and $M \geq 1.0\,M_\odot$, respectively. There is no significant mass segregation observed.

Figure 12. For each star and brown dwarf, we plot the magnitude of its velocity relative to the centre-of-mass velocity of the stellar system versus its distance from the most massive star in the cluster at the end of the main calculation. For binaries, the centre-of-mass velocity of the binary is given and the binary is plotted as a square rather than a circle. The velocity dispersion clearly depends on radius, with the outer regions having a significantly larger velocity dispersion. These outer objects have been ejected (see also Table 2).

centre increases (see Table 2 and Fig. 12). This is because only objects that have been ejected quickly can have made it out to these distances by the end of the calculation. Also, the binary fraction decreases outside of the 80 per cent mass radius. It drops by a factor of 2 between the 10 000–30 000 au (1–3 half-mass radii) radial bin and the 30 000–100 000 au (3–9 half-mass radii) bin, and there are no binaries (out of 41 objects) more than 100 000 au (>9 half-mass radii) from the cluster centre. Presumably, even though some binaries are ejected, they are less likely to be ejected than single objects, and the likelihood of them surviving the ejection process decreases with increasing ejection velocity (since a closer dynamical encounter is required to achieve a higher ejection velocity).

Observationally, the best cluster to compare our results to is the Orion Nebula Cluster (ONC). Hillenbrand & Hartmann (1998) examined its structure and dynamics. They estimated the stellar mass to be $\approx 2 \times 10^3\,M_\odot$ and the half-mass radius to be ≈ 0.8 pc, so the main simulation discussed here produces a cluster that is significantly less massive and more compact than the ONC. Although the ONC is larger and more massive, it is probably at a similar stage of evolution as the main calculation when it is stopped in the sense that it does not contain significant substructure (Bate, Clarke
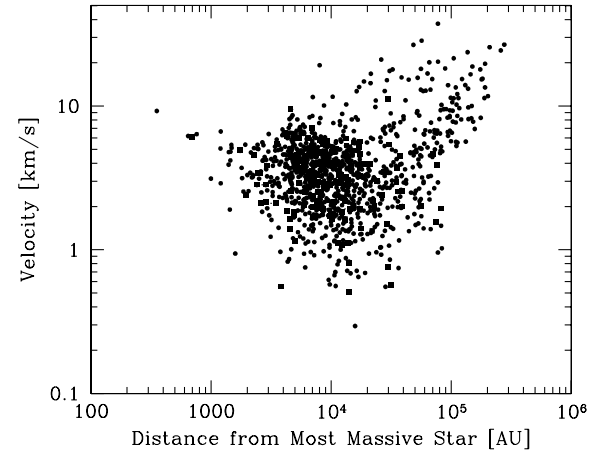
& McCaughrean 1998; Scally & Clarke 2002) and, if it was assembled from the merger of subclusters, the ONC's period of violent relaxation has ended. By contrast, the ρ Ophiuchi cloud contains a similar mass of stars and gas to the calculations presented here (Bontemps et al. 2001), but it is composed of many subclusters rather than a single large cluster.

Hillenbrand & Hartmann (1998) investigated mass segregation in the ONC and found that within the half-mass radius there was evidence for general mass segregation with stars in various mass bins becoming more centrally concentrated with increasing stellar mass. At larger radii, there was little evidence for mass segregation. At the end of the main calculation, we find no significant mass segregation. This is ironic since one of the main arguments usually advanced in favour of the competitive accretion model for star formation is that it naturally produces mass-segregated clusters (e.g. Bonnell et al. 1997, 2001). The difference here is most probably that the stellar cluster existing at the end of the main calculation has just formed from the merger of five subclusters, and even if these subclusters were mass-segregated before their mergers it is going to take some

time for the entire cluster to settle down again. This does illustrate that competitive accretion does not necessarily produce clusters that are mass-segregated throughout their entire formation process.

Köhler et al. (2006) investigated binarity in the ONC. They found that there was no significant dependence of the binary fraction on the distance from the cluster centre by comparing samples within ≈0.3 pc (approximately 40 per cent of the half-mass radius) of the centre with observations between 0.7 and 1.8 pc from the centre (approximately 1–2 half-mass radii). They stated that this was in contrast to the theory that the low binary frequency in the ONC compared to low-density star-forming regions was due to the dynamical disruption. However, their result is consistent with our hydrodynamical simulation, in that we also find no significant variation of binary fraction within three half-mass radii and binary disruption certainly occurs in the simulation. Only outside of three half-mass radii does there appear to be a slow decline in binarity. Needless to say, it would be interesting to try and detect a lower binary fraction or a higher velocity dispersion at distances more than three half-mass radii from the centre of the ONC to see whether the ONC displays variations like those apparent in the simulation. However, this would presumably be very difficult given the low stellar density and the problems of determining membership so far from the cluster centre.

3.3 Stellar encounters and disc sizes

Reipurth & Clarke (2001) proposed that brown dwarfs may be formed from dynamical ejections of low-mass objects from accreting unstable multiple systems, thus terminating their accretion and fixing them at low masses. Bate et al. (2002a), BBB2003, BB2005 and B2005 performed hydrodynamical simulations in which it was found that dynamical interactions were crucial in terminating accretion and setting an object's mass, but that this applied to stars as well as brown dwarfs (see also Section 3.1.2). Brown dwarfs were simply ejected soon after they had formed, while those objects ending up as stars suffered ejections only after a longer period of accretion.

Reipurth & Clarke (2001) also speculated that if brown dwarfs formed via ejection, they might have smaller, lower mass discs than stars. BBB2003, BB2005 and B2005 found that discs around stars and brown dwarfs were frequently truncated by dynamical encounters. However, some large discs were found to exist around both stars and brown dwarfs, while other stars and brown dwarfs had discs truncated to below the resolution limit of ≈10 au in their calculations.

In the calculations presented here, discs are resolved with radii down to ≈10 au in the main calculation and down to a few astronomical units in the rerun calculation. However, with SPH, the resolution length depends on density. Thus, for example, more massive discs are better resolved than low-mass discs. Furthermore, low-mass discs evolve much more quickly than high-mass discs due to the artificial viscosity present in the simulations (since the magnitude of the viscosity also depends on density). Because of these numerical effects, it is difficult to determine robustly the statistical properties of discs (e.g. their size and mass distributions).

By contrast, it is relatively simple to determine the closest dynamical encounter every star or brown dwarf has had during the calculation. In Fig. 13, we plot the distance of the closest encounter that every star and brown dwarf has had by the end of the main calculation. As in the earlier papers, there is a wide range of closest encounter distances, but stars have generally had closer encounters than brown dwarfs. However, this is somewhat misleading for sev-
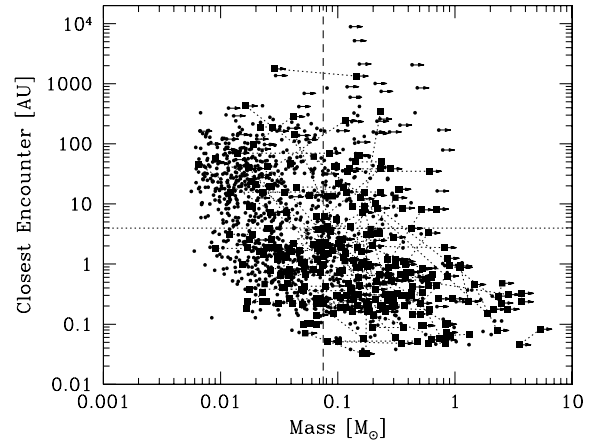

Figure 13. The closest encounter distances of each star or brown dwarf during the main calculation versus the final mass of each object. Objects that are still accreting significantly at the end of the calculation are denoted with arrows indicating that they are still evolving and that their masses are lower limits. Binaries are plotted with the two components connected by dotted lines and squares are used as opposed to circles. Encounter distances less than 4 au are upper limits since the point mass potential is softened within this radius. The vertical dashed line marks the star/brown dwarf boundary. The brown dwarfs in the top left-hand corner of the figure that are still accreting formed shortly before the calculation was stopped are thus still evolving rapidly. They may not end up as brown dwarfs.

eral reasons. First, as will be seen in the next section, multiplicity is a strong function of primary mass. In Fig. 13, it clear that (close) binaries are responsible for many of the 'closest encounters'. Secondly, objects that are still accreting at the end of the calculation are still evolving and, since the mass of an object depends on its 'age', more massive accreting objects are more likely to have had close encounters. In particular, most objects with brown dwarf masses that are still accreting have formed shortly before the calculation was stopped. They have not had much time for dynamical encounters to occur and may not end up as brown dwarfs. Finally, BBB2003, BB2005 and B2005 found that many stars that had close encounters still had resolved discs at the end of their calculations because those discs formed from accretion *subsequent* to their closest dynamical encounter.

Despite these difficulties, if an object suffers a dynamical encounter that terminates its accretion, this encounter will truncate any disc that is larger than approximately one-half of the periastron distance during the encounter (Hall, Clarke & Pringle 1996). Therefore, excluding binaries and objects that are still accreting, determining the distribution of one-half of the closest encounter distance should give us an indication of the disc size distribution around single objects that have reached their final masses. Note that formally we have still included the wide components of triple and quadruple systems, but these constitute only 48 objects out of the 884 'single' non-accreting objects, so should not adversely affect any conclusions.

In Fig. 14, we plot the cumulative distributions of disc truncation radii (taken to be one-half of the closest encounter distance) for these objects. The solid line gives the cumulative distribution for all 884 objects, while in the other distributions we break the sample into mass bins of $M < 0.1, 0.1 \leq M < 0.3, 0.3 \leq M < 1.0$ and $M \geq 1.0\,M_{\odot}$. More massive stars tend to have had closer encounters and, thus, have smaller disc truncation radii. The median truncation radius is two orders of magnitude larger for the VLM objects than
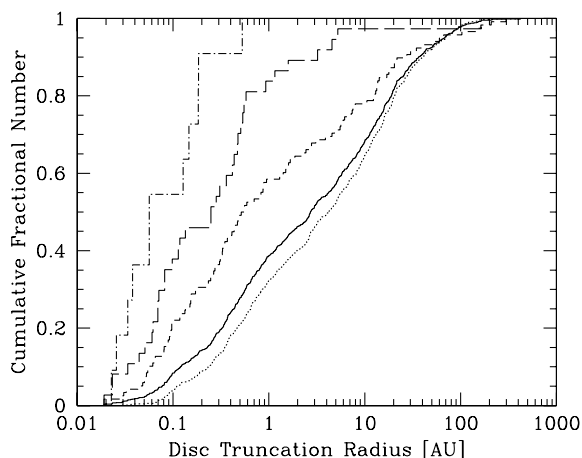
Figure 14. Due to dynamical interactions, stars and brown dwarfs *potentially* have their discs truncated to approximately one-half of the periastron separation during the encounter (see also Fig. 13). At the end of the main calculation, we plot the cumulative fraction objects as a function of the potential truncation radius. We exclude binaries and any objects that are still accreting at the end of the calculation. The solid line gives the result for all stars and brown dwarfs, while the dotted, short-dashed, long-dashed and dot–dashed lines give the cumulative distributions for the mass ranges $M < 0.1$, $0.1 \leq M < 0.3$, $0.3 \leq M < 1.0$ and $M \geq 1.0\,\mathrm{M}_\odot$, respectively. More massive stars tend to have had closer encounters.

for the solar-type stars. In particular, we note that 10 per cent of the VLM stars have truncation radii greater than 40 au, while one-third have truncation radii greater than 10 au.

We emphasize that Fig. 14 should be used with caution. First, the simulation presented here produces a very dense stellar cluster. Disc truncation may be less important for setting disc sizes in a lower density star-forming region. Secondly, Fig. 14 does *not* give a disc size distribution. At best, it is a distribution of *lower limits* to disc sizes because of the fact that stars can suffer a close dynamical encounter, but then accrete more material from the molecular cloud and form a new disc. This happens frequently in the simulation, especially for the higher-mass stars. The distribution is likely to be most useful for VLM objects because they tend to have their accretion terminated soon after they form by dynamical encounters and generally will not subsequently accrete significantly from the molecular cloud.

Armitage, Clarke & Palla (2003) considered the lifetimes of circumstellar discs surrounding young stars. They obtained a good fit to the observed distributions of lifetimes with a 1σ dispersion of 0.5 dex in the initial disc masses, with the exception of the ≈30 per cent of young weak-lined T-Tauri stars (WTTS) that appeared to have lost their discs even with an age of 1 Myr. There are two points of interest here. First, we note that the dispersion of the time-averaged accretion rates for an object of a given final mass (Section 3.1.2 and Fig. 7) is 0.4 dex in the main calculation (and similar values were obtained by BBB2005 and B2005). This might naturally be expected to lead to the dispersion in disc masses that Armitage et al. required to explain the disc lifetime distributions. Secondly, we find that many objects have had very close dynamical encounters. For some objects, their closest encounters will be the one that ejects them from the stellar group they are formed in. Once they are ejected, it is unlikely they will accrete a new disc. Such objects might help to explain the observation that some WTTS appear to have lost their discs at a very young age (see also Armitage & Clarke 1997).

3.4 Multiplicity as a function of primary mass

We turn now to the properties of the binary and higher-order multiple stars and brown dwarfs produced by the simulations. The properties of multiple stellar systems have been investigated in the past through ensembles of small *N*-body (e.g. McDonald & Clarke 1993, 1995; Sterzik & Durisen 1998, 2003; Hubber & Whitworth 2005) or hydrodynamical (e.g. Delgado-Donate et al. 2004; Goodwin et al. 2004b,c) simulations, with some of the observed trends in properties being reproduced depending on the input parameters. However, this is the first time a large number of multiple stars and brown dwarfs have been produced from a single hydrodynamical simulation of star formation. Although the calculation produces more brown dwarfs than is realistic, it is still of great importance to compare the multiple systems with the observations. It may be, for example, that precisely modelling the IMF requires radiative transfer to be included, but that some binary properties do not depend significantly on whether radiative transfer is included or not.

Observationally, it is clear that the fraction of stars or brown dwarfs that are in multiple systems increases with stellar mass (massive stars: Mason et al. 1998; Preibisch et al. 1999, intermediate-mass stars: Patience et al. 2002, solar-type stars: Duquennoy & Mayor 1991, M dwarfs: Fischer & Marcy 1992 and VLM stars and brown dwarfs: Close et al. 2003; Siegler et al. 2005; Basri & Reiners 2006). It also seems that the multiplicity of young stars in low-density star-forming regions is somewhat higher than that of field stars (Ghez, Neugebauer & Matthews 1993; Leinert et al. 1993; Simon et al. 1995; Duchêne et al. 2007). However, IC 348 has a similar binary frequency to the field (Duchêne, Bouvier & Simon 1999). In the ONC, Köhler et al. (2006) find that the binary frequency of low-mass stars is similar to that of field M dwarfs and lower than that of field solar-type stars, but that stars with masses $M > 2\,\mathrm{M}_\odot$ have a higher binarity than stars with $0.1 < M < 2\,\mathrm{M}_\odot$ by a factor of 2.4 to 4.

To quantify the fraction of stars and brown dwarfs that are in multiple systems, we use the multiplicity fraction (MF) defined as a function of stellar mass. We define this as

$$\mathrm{MF} = \frac{B + T + Q}{S + B + T + Q}, \qquad (2)$$

where S is the number of single stars within a given mass range and B, T and Q are the numbers of binary, triple and quadruple systems, respectively, for which the primary has a mass in the same mass range. Note that this differs from the companion star fraction (CSF), that is also often used and where the numerator has the form $B + 2T + 3Q$. We choose the multiplicity fraction following Hubber & Whitworth (2005), who point out that this measure is more robust observationally in the sense that if a new member of a multiple system is found (e.g. a binary is found to be a triple), the quantity remains unchanged. We also note that it is more robust for simulations too in the sense that if a high-order system decays because it is unstable, the numerator only changes if a quadruple decays into two binaries (which is quite rare). Furthermore, if the denominator is much larger than the numerator (e.g. for brown dwarfs where the multiplicity fraction is low), the production of a few single objects does not result in a large change in the value of MF. This is useful because many of the systems in existence at the end of the calculations presented here may undergo further dynamical evolution. By using the multiplicity fraction, our statistics are less sensitive to this later evolution.

When analysing the simulations, some subtleties arise. For example, many 'binaries' are in fact members of triple or quadruple

Table 3. The numbers of single and multiple systems for different primary mass ranges at the end of the main calculation. In the lower portion of the table, the numbers exclude brown dwarf ($M < 0.075\,M_\odot$ companions) to allow better comparison with the surveys of Duquennoy & Mayor (1991) and Fischer & Marcy (1992) which were not sensitive to brown dwarfs (e.g. a solar-type star with any number of brown dwarf companions would be counted as a single solar-type star, while a solar-type star with a close brown dwarf companion and a wide M-star companion would be counted as a solar-type binary).

Mass range [$M_\odot$]	Single	Binary	Triple	Quadruple
$M < 0.01$	82	0	0	0
$0.01 \leq M < 0.03$	348	8	1	0
$0.03 \leq M < 0.07$	207	18	2	0
$0.07 \leq M < 0.10$	78	6	1	2
$0.10 \leq M < 0.20$	99	22	4	2
$0.20 \leq M < 0.50$	59	23	5	10
$0.50 \leq M < 0.80$	16	7	4	4
$0.80 \leq M < 1.2$	7	3	3	3
$M > 1.2$	9	3	3	4
All masses	905	90	23	25
$0.10 \leq M < 0.20$ (no BD)	116	15	0	1
$0.20 \leq M < 0.50$ (no BD)	66	25	8	1
$0.50 \leq M < 0.80$ (no BD)	18	10	3	1
$0.80 \leq M < 1.2$ (no BD)	8	5	3	0
$M > 1.2$ (no BD)	12	4	3	0

systems, and some 'triple' systems are components of quadruple or higher-order systems. From this point onwards, unless otherwise stated, we define the numbers of multiple systems as follows. The number of binaries excludes those that are components of triples or quadruples. The number of triples excludes those that are members of quadruples. However, higher-order systems are ignored (e.g. a quintuple system may consist of a triple and a binary in orbit around each other, but this would be counted as one binary and one triple). We need to stop counting larger and larger multiple systems at some point because in fact the simulation forms one large cluster to which many of the multiple systems are still bound when the calculation is finished (see Section 2.2.1 for a description of

how we identify multiple systems). We choose quadruple systems as a convenient point to stop, as it is likely that most higher-order systems would decay if the cluster was evolved for many millions of years. The numbers of single and multiple stars produced by the main hydrodynamical calculation are given in Table 3 following these definitions.

In Fig. 15, we plot the multiplicity fraction of the stars and brown dwarfs as a function of the primary mass for the main calculation, based on the numbers given in Table 3. In the left-hand panel, we divide the objects into low-mass brown dwarfs (masses <30 Jupiter masses or $0.03\,M_\odot$), VLM objects excluding the low-mass brown dwarfs (masses 0.03–$0.10\,M_\odot$), low-mass stars (masses 0.10–$0.80\,M_\odot$), solar-type stars (masses 0.80–$1.20\,M_\odot$) and intermediate-mass stars (masses $>1.2\,M_\odot$). In the right-hand panel, finer mass divisions are used for masses less than $0.8\,M_\odot$. These divisions are chosen for comparison with various observational surveys. In Fig. 15, the filled blue squares give the multiplicity fraction, while the surrounding blue-hatched regions give the range in primary masses over which the fraction is calculated and the 1σ (68 per cent) uncertainty on the multiplicity fraction (e.g. for solar-type primary stars, the multiplicity fraction is 0.56 ± 0.12). The black open boxes and their associated error bars and/or upper/lower limits give the results from a variety of observational surveys (see the figure caption). Finally, in the right-hand panel, the filled red squares and their associated red-hatched regions give the multiplicity fractions excluding brown dwarfs (masses less than $0.075\,M_\odot$).

The main hydrodynamical calculation clearly predicts that the multiplicity fraction strongly increases with increasing primary mass. Furthermore, the values in each mass range are in reasonable agreement with observation. There is excellent agreement for solar-type and low-mass stars. For intermediate-mass stars, the statistics from the calculation are poor (and the observed value is also uncertain), while for VLM objects, the hydrodynamical calculation gives a slightly lower prediction than the observations, but not unreasonably so.

In detail, we find the following.

Solar-type stars. Duquennoy & Mayor (1991) find an observed multiplicity fraction of 0.58 ± 0.1. The main calculation gives a multiplicity fraction of 0.56 ± 0.12. However, this figure includes brown dwarf companions and Duquennoy & Mayor's
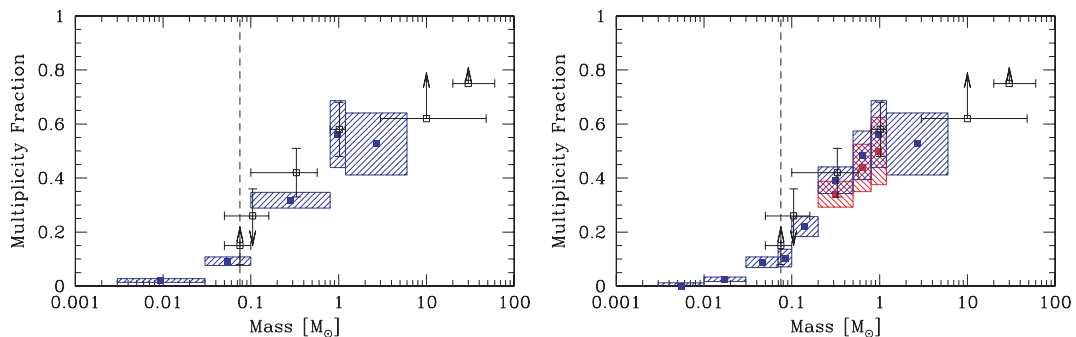

Figure 15. Multiplicity fraction as a function of primary mass. The left- and right-hand panels both give results from the main calculation, but different mass ranges are used for the low-mass stars. On the right, the mass ranges are those given in the upper section of Table 3, while on the left only three mass ranges are used for objects with masses $M < 0.8\,M_\odot$ (namely, $M < 0.03$, $0.03 \leq M < 0.1$ and $0.1 \leq M < 0.8\,M_\odot$). The blue filled squares surrounded by shaded regions give the results from the main calculation with their statistical uncertainties. The open black squares with error bars and/or upper/lower limits give the observed multiplicity fractions from the surveys of Close et al. (2003), Basri & Reiners (2006), Fischer & Marcy (1992), Duquennoy & Mayor (1991), Preibisch et al. (1999) and Mason et al. (1998), from left to right in each panel. The red filled squares and associated shaded regions in the right-hand panel give the multiplicity fractions excluding brown dwarf companions (masses $<0.075\,M_\odot$) to allow better comparison with the surveys of Duquennoy & Mayor and Fischer & Marcy. The general trend of increasing multiplicity with primary mass is well reproduced by the main calculation. Note that because the multiplicity is a steep function of primary mass, it is important to ensure that similar mass ranges are used when comparing the simulation with observations.

survey was not sensitive to brown dwarfs. Excluding them, we obtain 0.50 ± 0.13 which is still in good agreement with the observed value.

M dwarfs. Fischer & Marcy (1992) find an observed multiplicity fraction of 0.42 ± 0.09. In the mass range 0.1–$0.8\,M_\odot$, we obtain $MF = 0.32 \pm 0.03$ which is slightly lower than the observed value, though still within the uncertainties. However, in this mass range the multiplicity fraction changes quite rapidly with mass. Fischer & Marcy's sample contains stars with masses between 0.1 and 0.57 solar masses, but the vast majority have masses in the range $0.2 - 0.5\,M_\odot$, whereas in the hydrodynamical simulation around half of the low-mass stars have masses less than $0.2\,M_\odot$. In the 0.2–$0.5\,M_\odot$ mass range, we obtain $MF = 0.39 \pm 0.05$. However, Fischer & Marcy's survey was also not sensitive to brown dwarf companions. Removing these, we obtain 0.34 ± 0.05. This value is consistent with the observed value, lying well within the 1σ uncertainties.

VLM objects. There has been much interest in the multiplicity of VLM objects in recent years (Martín et al. 2000, 2003; Bouy et al. 2003, 2006; Close et al. 2003, 2007; Gizis et al. 2003; Pinfield et al. 2003; Siegler et al. 2003, 2005; Luhman 2004; Kraus, White & Hillenbrand 2005, 2006; Maxted & Jeffries 2005; Basri & Reiners 2006; Reid et al. 2006; Ahmic et al. 2007; Allen et al. 2007; Konopacky et al. 2007; Law, Hodgkin & Mackay 2008; Maxted et al. 2008; Reid et al. 2008). For a recent review, see Burgasser et al. (2007). Over the entire mass range of 0.003–$0.10\,M_\odot$, we find a very low multiplicity of just 0.047 ± 0.008. We note the main calculation, which is essentially a larger version of the calculation reported in BBB2003, produces a VLM object multiplicity in agreement with the earlier, smaller calculations which gave $MF \approx 0.06$ (B2005). However, in the earlier calculations it was impossible to subdivide the VLM objects because of the small numbers. As with the M dwarfs, the multiplicity drops rapidly with decreasing primary mass, and the *observed* VLM objects tend to have high masses. The main calculation gives multiplicities of 0.22 ± 0.04 for the mass range 0.1–$0.2\,M_\odot$, 0.10 ± 0.03 for the mass range 0.07–$0.10\,M_\odot$, 0.09 ± 0.02 for the mass range 0.03–$0.07\,M_\odot$, 0.025 ± 0.008 for the mass range 0.01–$0.03\,M_\odot$ and 0.00 ± 0.01 for masses less than $0.01\,M_\odot$. Therefore, to compare with observations, it is very important to compare like with like. The observed frequency of VLM binaries is typically found to be ≈ 15 per cent (Bouy et al. 2003; Close et al. 2003, 2007; Gizis et al. 2003; Martín et al. 2003; Siegler et al. 2005; Reid et al. 2008). The surveys are most complete for binary separations greater than a couple of astronom-

ical units. Recently, Basri & Reiners (2006) estimated the total frequency (including spectroscopic systems) to be ≈ 20–25 per cent. These surveys typically targeted primaries with masses in the range 0.03–$0.1\,M_\odot$, but most of these objects in fact have masses greater than $0.07\,M_\odot$. Thus, the closest comparison with our calculation is our frequency of 0.10 ± 0.03 for the mass range 0.07–$0.10\,M_\odot$. This is somewhat lower than the observed frequency (a factor of 2 at face value), but still in better agreement than that from the earlier simulations (B2005). In the next section, we show that decreasing the accretion radii of the sink particles increases the frequency of VLM binaries bringing them into good agreement with the observed value. Thus, the main calculation produces a VLM binary frequency that is consistent with observations (at around 2–3σ level), but it is lower and we attribute this to the effects of the sink particle approximation rather than a fundamental failing of the hydrodynamical star formation model.

Low-mass brown dwarfs. The frequency of low-mass binary brown dwarfs (primary masses less than 30 Jupiter masses) is observationally unconstrained. *We predict that the multiplicity continues to fall as the primary mass is decreased as described above.* Even if our predicted multiplicities are underestimated by a factor of 2 or even 3 due to the effects of sink particles, we would predict that the binary frequency in the mass range of 0.01–$0.03\,M_\odot$ is $\lesssim 7$ per cent. Companions to brown dwarfs with masses less than 10 Jupiter masses should be exceptionally rare ($\lesssim 3$ per cent).

3.4.1 The dependence of multiplicity on sink particle approximations

As with the IMF, the question arises on how dependent these results are on the use of sink particles. In particular, in the main calculation, binaries cannot have separations smaller than 1 au (due to the gravitational softening), and the sink particle accretion radius removes all gas within 5 au of the sink particle, presumably affecting close dynamical interactions between protostellar objects. This is likely to have a severe effect on the properties of short-period binaries. As mentioned above and will be seen in more detail in Section 3.3, this particularly affects the VLM binaries whose median separation in the main calculation (and observationally) is less than 10 au.

In Fig. 16, we compare the multiplicity fractions produced by the main calculation (left-hand panel) and the rerun calculation (right-hand panel) at the end time of the rerun calculation ($t_{\rm ff} = 1.038$). The first point to note is that the fractions given by the main calculation
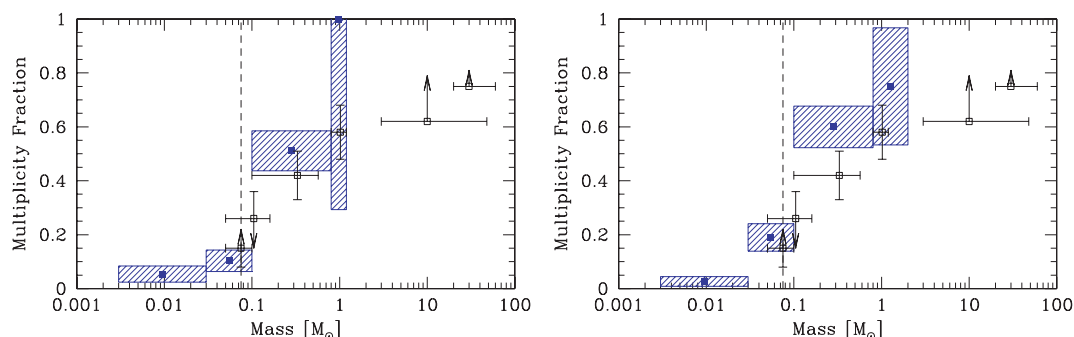

Figure 16. Multiplicity fraction as a function of primary mass for the main calculation at $t = 1.038t_{\rm ff}$ (left-hand panel) and the rerun calculation at the same time (right-hand panel). The blue filled squares surrounded by shaded regions give the results from the calculations. The open black squares with error bars and/or upper/lower limits give the observed multiplicity fractions from the surveys of Close et al. (2003), Basri & Reiners (2006), Fischer & Marcy (1992), Duquennoy & Mayor (1991), Preibisch et al. (1999) and Mason et al. (1998), from left to right in each panel. The multiplicities for primaries with masses in the range 0.03–$0.8\,M_\odot$ are higher in the rerun calculation in which the sink particles have smaller accretion radii and no gravitational softening.

at 1.038 and 1.50t_{ff} are the same within the statistical uncertainties. Therefore, we conclude that the fractions do not evolve significantly with time (though their mass ratios and separations might – see Sections 3.5 and 3.6). There are few stars with masses greater than 0.8 $M_{\odot}$ at the earlier time because they have not yet had time to accrete to high masses. Thus, the multiplicity fractions of solar-type and intermediate-mass stars are poorly defined. However, for low-mass stars, the fractions are 0.51 ± 0.07 and 0.32 ± 0.03, respectively, which lie within 2σ of each other. For VLM systems, the fractions are 0.10 ± 0.04 and 0.092 ± 0.016, respectively. For low-mass brown dwarfs, the fractions are 0.054 ± 0.030 and 0.021 ± 0.007, respectively.

We now compare the fractions given by the main calculation and the rerun calculation, the latter of which has smaller sink particle accretion radii (left- and right-hand panels of Fig. 16). The multiplicity fractions are greater in the rerun calculation for VLM objects and low-mass stars, but not for the low-mass brown dwarfs. An increase in the multiplicity fractions for small sink particles is what we might expect since binaries can become tighter (due to the absence of gravitational softening) and dissipative processes can play a role on smaller scales (due to the smaller accretion radii of only 0.5 au). Low-mass stars in the rerun calculation have a multiplicity of 0.60 ± 0.08, which differs by ≈0.6σ from the main calculation at the same time. VLM binaries have a multiplicity of 0.19 ± 0.05. This is 1σ higher than the main calculation at the same time. Finally, low-mass brown dwarfs have a multiplicity of 0.026 ± 0.018 which differs by 0.6σ from the main calculation at the same time.

Clearly, even with such large numbers of objects, statistical uncertainties still make comparison of the results difficult. However, the indication is that decreasing the sizes of the sink particles increases the multiplicity fractions, at least for the mass range 0.03–0.80 $M_{\odot}$. In particular, decreasing the sizes of the sink particles maintains the good agreement with observations for solar-type and low-mass stars, and improves the agreement for VLM objects. The multiplicity of 19 ± 5 per cent for the mass range 0.03–0.10 $M_{\odot}$ is in excellent agreement with the typically observed value of ≈15 per cent (Close et al. 2003) and the upper limit of 20–25 per cent estimated by Basri & Reiners (2006).

In summary, it seems that *purely hydrodynamical simulations of star formation using sink particles can reproduce the observed multiplicities of solar-type stars, low-mass stars and VLM objects.* The results appear to depend slightly on the sink particle assumptions, with smaller sink particles generally leading to slightly higher multiplicities and better agreement with observations.

3.4.2 Star–VLM binaries

We turn now to the issue of VLM/brown dwarf companions to stars. As in the previous section, we do not consider brown dwarf companions as such, rather we consider VLM companions (<0.1 $M_{\odot}$) to stars (≥0.1 $M_{\odot}$). The main calculation produced 26 stellar-VLM binaries out of 290 stellar systems, a frequency of 9.0 ± 1.6 per cent. For the vast majority of these stellar-VLM binaries, the star is a low-mass star: 14 of the primaries have masses between 0.1 and 0.2 $M_{\odot}$, seven have primary masses in the range 0.2–0.5 $M_{\odot}$ and three have primary masses between 0.5 and 0.8 $M_{\odot}$. However, within the statistical uncertainties, the frequency of VLM companions is not found to depend on primary mass. Even around solar-type and intermediate-mass stars we find VLM companions, but the statistics are very poor with only two out of the 35 systems with pri-

mary masses greater than 0.8 $M_{\odot}$ being star/VLM binaries (6 ± 4 per cent).

Although there is no statistically significant dependence of the frequency of such systems on primary mass, the separation distributions are very different. For primaries with masses of 0.1–0.2 $M_{\odot}$, the semimajor axes of all but three of the 14 systems are less than 30 au. The other three all have semimajor axes greater than 1000 au. This separation distribution is very similar to the VLM and brown dwarf binaries discussed in Section 3.5. For the seven primaries with masses of 0.2–0.5 $M_{\odot}$, three have VLM companions within 10 au, there is one at 49 au and the remaining three have wide companions (greater than 1000 au). The VLM companions of the three primaries with masses of 0.5–0.8 $M_{\odot}$ have semimajor axes between 27 and 65 au. Finally, the two star/VLM binaries with primary masses greater than 0.8 $M_{\odot}$ both have semimajor axes greater than 1000 au. Thus, *the typical separation of star/VLM binaries seems to increase strongly as the mass of the primary increases.*

In addition to the star/VLM binaries, there are four triple systems consisting of a star with two VLM companions and eight quadruple systems that contain at least one star/VLM pair. In all but three of these 12 systems, the widest orbit has a semimajor axis in the range 50–500 au. The remaining three systems have very wide outer orbits (>1000 au).

There has been much discussion over the past decade about the observed 'brown dwarf desert' for close brown dwarf companion solar-type stars (frequency ≈1 per cent; Marcy & Butler 2000; Grether & Lineweaver 2006) and how this changes for wider separations and different primary masses. McCarthy & Zuckerman (2004) found that the frequency of wide brown dwarfs to G, K and M stars between 75 and 300 au was 1 ± 1 per cent. The frequencies of wide brown dwarf companions to A and B stars (Kouwenhoven, Brown & Kaper 2007), M dwarfs (Gizis et al. 2003) and other brown dwarfs appear to be similarly low, although the frequency of wide binary brown dwarfs may be higher when they are very young (Close et al. 2007). Our results are consistent with these observations in the sense that we do not find brown dwarf companions to solar-type stars in close orbits (frequency ≲8 per cent at the 95 per cent confidence level), but that VLM companions exist orbiting stars and brown dwarfs with a wide range of masses. Our results are also in good agreement with surveys of VLM objects that are frequently found to have companions, but where their separations are usually less than ≈20 au (Close et al. 2003, 2007; Allen et al. 2007). It would be of great interest to map out the separation distributions of VLM companions over a wide range of primary masses. From the results of the main calculation, we predict that the frequency of star–brown dwarf systems should not depend greatly on primary mass, but that the typical star–brown dwarf binary separation should increase monotonically from ≲10 au for primary masses less than 0.2 $M_{\odot}$ to ~50 au for primary masses ~0.4 $M_{\odot}$ and to >100 au for solar-type stars.

3.4.3 The frequencies of triple and quadruple systems

Consulting Table 3, we find that the main calculation produced 905 single stars/brown dwarfs, 90 binaries, 23 triples and 25 quadruples. This gives an overall frequency of triple and quadruple systems of only 2.3 ± 0.5 and 2.5 ± 0.5 per cent, respectively. These are upper limits because some of these systems may be disrupted if the calculation were followed longer.

Although the overall frequencies are low, it is clear from the table that the frequencies of high-order multiples depend strongly on

primary mass. For VLM primaries, the frequencies of triple/quadruple systems range from 3.4 ± 2.0 per cent for the mass range 0.07–$0.10 \, M_\odot$ to 0.9 ± 0.6 per cent for 0.03–$0.07 \, M_\odot$ and much less than 1 per cent for lower primary masses. For low-mass M stars in the range 0.10–$0.20 \, M_\odot$, the frequency of triples/quadruples is 5 ± 2 per cent. For M stars with masses in the range 0.20–$0.50 \, M_\odot$, the frequency of triples/quadruples is 15 ± 4 per cent, while for solar-type and intermediate-mass stars the frequency is $\approx 37 \pm 12$ per cent.

How do these frequencies compare with observations? Fischer & Marcy (1992) find seven triples and one quadruple amongst 99 M-star primaries giving a frequency of 8 ± 3 per cent. As mentioned earlier, Fischer and Marcy's survey was not sensitive to brown dwarf companions, and most of their M stars had masses in the range 0.2–$0.5 \, M_\odot$. Excluding brown dwarfs from the multiple statistics, we find a frequency of 9 ± 3 per cent for this stellar mass range in excellent agreement. Duquennoy & Mayor (1991) found seven triples and two quadruples from their 164 solar-type primaries giving a frequency of 5 ± 2 per cent. For solar-type stars (excluding brown dwarf companions), we find a frequency of 18 ± 10 per cent. The large uncertainty in our result makes comparison difficult for the solar-type stars, but our result is not unreasonable, especially given the fact that Duquennoy & Mayor admit that they are likely to have missed some high-order multiple systems.

In summary, our frequencies of triples/quadruples are consistent with the current observational surveys, though more robust statistics from observations, particularly for VLM objects, and improved statistics from the simulations, particularly for intermediate-mass stars, are obviously desirable.

3.5 Separation distributions of multiples

With 58 stellar and 32 VLM binaries we can, for the first time, study the properties of a reasonably large sample of binary systems formed in a single star cluster. The main calculation also produced 19 stellar and four VLM triple systems, and 23 stellar and two VLM quadruple systems.

Observationally, the median separation of binaries is found to depend on primary mass. Duquennoy & Mayor (1991) found that the median separation of solar-type binaries was ≈ 30 au. Fischer & Marcy (1992) found indications of a smaller median separation of ≈ 10 au for M-dwarf binaries. Finally, VLM binaries are found to have a median separation of $\lesssim 4$ au (Close et al. 2003, 2007; Siegler et al. 2005), with very few VLM binaries found to have separations greater than 20 au, particularly in the field (Allen et al. 2007). Most recently, Close et al. (2007) estimated that young VLM objects have a wide (>100 au) binary frequency of $\sim 6 \pm 3$ per cent for ages less than 10 Myr, but only 0.3 ± 0.1 per cent for field VLM objects.

Unfortunately, in the main calculation, the gravitational force between sink particles is softened when they approach within 4 au with the maximum acceleration, and hence the minimum binary separation, occurring at 1 au. Furthermore, gas within 5 au of a sink particle is accreted, meaning that dissipative interactions with the gas are omitted on these scales. These numerical approximations necessarily affect the formation of the multiple systems. In the rerun calculation, no gravitational softening is applied and binaries with separations as small as 0.02 au could be produced. However, the sink particles still accrete gas within 0.5 au, which is likely to affect the binary formation, and smaller numbers of multiple systems are produced in the rerun calculation giving poorer statistics.

In Fig. 17, we present the separation (semimajor axis) distributions of the stellar (primary masses greater than $0.10 \, M_\odot$) and VLM multiples. These distributions are compared with the surveys of Duquennoy & Mayor (1991), Fischer & Marcy (1992) and the listing of VLM multiples maintained by Nick Siegler at http://vlmbinaries.org/, respectively. The filled histograms give the separations of binary systems, while the double-hashed region adds the separations from triple systems (two separations for each triple, determined by subdividing the triple into a binary with a wider
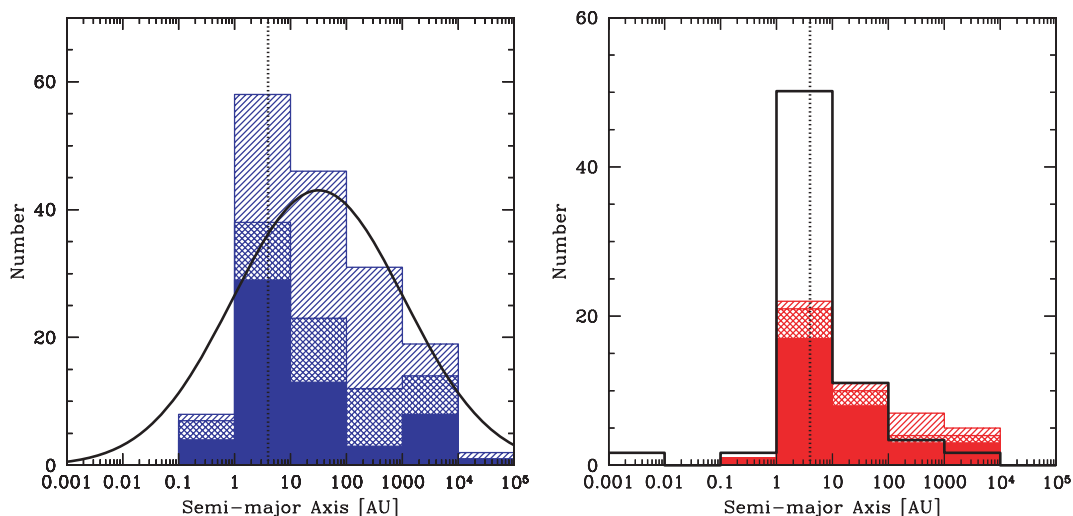

Figure 17. The distributions of separations (semimajor axes) of multiple systems with stellar (left-hand panel) and VLM (right-hand panel) primaries produced by the main calculation. The solid, double-hashed and single-hashed histograms give the orbital separations of binaries, triples and quadruples, respectively (each triple contributes two separations and each quadruple contributes three separations). In the stellar graph, the curve gives the G-dwarf separation distribution (scaled to match the area) from Duquennoy & Mayor (1991). In the VLM systems graph, the open black histogram gives the (scaled to match the number in the 10–100 au range) separation distribution of the known VLM multiple systems maintained by Nick Siegler at http://vlmbinaries.org/ (last updated on 2008 February 4). The vertical dotted line gives the resolution limit of the calculations as determined by the gravitational softening and accretion radii of the sink particles.

companion), and the single-hashed region includes the separations of quadruple systems (three separations for each quadruple which may be composed of two binary components or a triple with a wider companion).

We find that in the main calculation, the median separation (including separations from binary, triple and quadruple systems) increases with increasing primary mass. The stellar systems have a median separation of 26 au, while the VLM systems have a median separation of 10 au. These values are in reasonable agreement with the observed values mentioned above, and the shapes of the separations distributions for stellar and VLM primaries are satisfactory (at least beyond 10 au). However, it is also clear from Fig. 17 that the resolution limits imposed by the sink particle approximations (vertical dotted lines) almost certainly affect the distributions since the peaks of both the stellar and the VLM distributions occur in the 1–10 au separation bin.

To investigate the effects of the sink particle approximations on the distributions, in Fig. 18, we display the stellar and VLM separation distributions from the rerun calculation (lower panels) and the main calculation at the same time ($t = 1.038\ t_{ff}$;

upper panels). As expected, reducing the sink particle accretion radii and gravitational softening produces closer multiple systems. The effect on the stellar distribution is particularly pleasing in that the separation distribution becomes more bell like and the peak occurs in the 10–100 au bin (rather than the 1–10 au bin) which is well separated from the resolution limit (vertical dotted line).

More VLM multiple systems are formed in the rerun calculation, and there are more with separations of <10 au. Of even more interest is the fact that, at $t = 1.038\ t_{ff}$, the median separations of the VLM multiples in the main calculation and the rerun calculation are similar to each other and to the stellar multiples, but much larger than at the end of the main calculation (≈ 30 au at early times, but ≈ 10 au at the end of the main calculation). Admittedly, the smaller numbers of VLM multiples at early times means that the uncertainties are large. However, this indicates that *VLM systems may form with reasonably wide separations and evolve to smaller separations.* We note that at $t = 1.038 t_{ff}$, two-thirds of the VLM multiples in the main calculation and more than 80 per cent of those in the rerun calculation are still accreting (and, thus, still
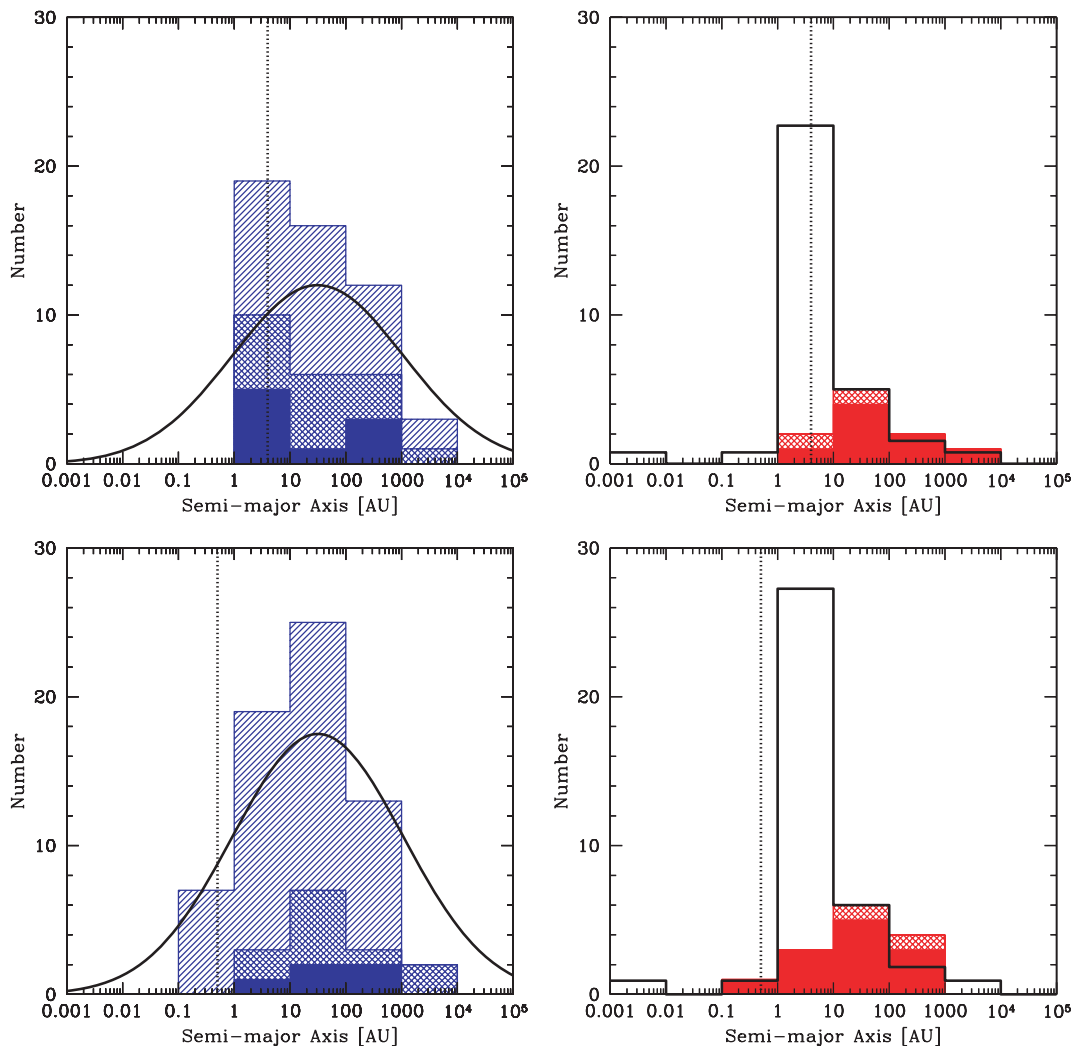
Figure 18. Same as Fig. 17 but the separation (semimajor axis) distributions are given at $t = 1.038\ t_{ff}$ for the main calculation (top panels) and the rerun calculation which uses sink particles with small accretion radii (0.5 au) and without gravitational softening (bottom panels). As expected, reducing the lengthscales of the sink particle accretion radii and gravitational softening produces a higher fraction of small-separation multiple systems. In addition, the 'pile up' of stellar system separations in the 1–10 au bin (top left-hand panel) disappears when smaller separations are allowed (bottom left-hand panel), recovering a bell-shaped distribution more similar to the observed Duquennoy & Mayor (1991) distribution for solar-type primaries.

evolving), whereas at the end of the main calculation, all but one VLM multiple has ceased accreting. Bate et al. (2002b) discuss how close binaries (separations less than 10 au) are formed from wider systems in the BBB2003 calculation through a combination of dynamical encounters with other protostars, their interactions with circumbinary and circumtriple discs and accretion. Since the main calculation is simply a larger version of BBB2003's calculation, it is probable that such evolution is also occurring here. The possibility of VLM binaries undergoing evolution has also been suggested observationally. Close et al. (2007) and Burgasser et al. (2007) suggest that young, wide, VLM binaries are disrupted, leading to the observed paucity of old, wide, VLM systems. They also find evidence that a higher proportion of young VLM systems may have unequal-mass components than for older systems (see also the next section).

3.6 Mass ratio distributions of binaries

Along with the separation distributions of the multiple systems, we can investigate the mass ratio distributions. In this section, we only consider binaries, but we include binaries that are components of triple and quadruple systems. A triple system composed of a binary with a wider companion contributes the mass ratio from the binary, as does a quadruple composed of a triple with a wider companion. A quadruple composed of two binaries orbiting each other contributes two mass ratios – one from each of the binaries.

Observationally, the mass ratio distribution of binaries is also found to depend on primary mass. Duquennoy & Mayor (1991) found that the mass ratio distribution of solar-type binaries peaked at $M_2/M_1 \approx 0.2$. Halbwachs et al. (2003) found a bimodal distribution for spectroscopic binaries with primary masses in the mass range 0.6–$1.9\,M_\odot$ and periods $\lesssim 10$ yr with a broad peak in the range $M_2/M_1 = 0.2$–0.7 and a peak for equal-mass systems (so-called twins; Tokovinin 2000b). They also noted that the frequency of twins was higher for periods <100 d, though this is not relevant for the calculations presented here since they do not probe such short periods. Mazeh et al. (2003) found a flat mass ratio distribution for spectroscopic binaries with primaries in the mass range 0.6–$0.85\,M_\odot$. Fischer & Marcy (1992) also found a flat mass ratio distribution in the range $M_2/M_1 = 0.4$–1.0 for M-dwarf binaries

with all periods. Finally, VLM binaries are found to have a strong preference for equal-mass systems (Close et al. 2003; Siegler et al. 2005; Reid et al. 2006).

In Fig. 19, we present the mass ratio distributions of the stars with masses $\geq 0.5\,M_\odot$ (left-hand panel), M dwarfs with masses $0.1 \leq M < 0.5\,M_\odot$ (centre panel) and VLM objects (right-hand panel). We compare the M-dwarf mass ratio distribution to that of Fischer & Marcy (1992), and the higher-mass stars to the mass ratio distribution of solar-type stars obtained by Duquennoy & Mayor (1991). The VLM mass ratio distribution is compared with the listing of VLM multiples maintained by Nick Siegler at http://vlmbinaries.org/.

We find that in the main calculation, the ratio of near-equal-mass systems to systems with dissimilar masses decreases going from VLM objects to M dwarfs in a similar way to the observed mass ratio distributions, but that the trend is not as strong as in the observed systems. Specifically, 71 per cent of the VLM binaries have $M_2/M_1 > 0.6$ while for primary masses 0.1–$0.5\,M_\odot$, the fraction is only 51 per cent. The stellar mass ratio distribution is consistent with Fischer & Marcy's distribution. The VLM binaries, although biased towards equal-mass systems, are not as strongly biased as is observed. However, currently there is no volume-limited sample for VLM systems, and systems with more equal-mass components are easier to detect, so the degree to which the observed mass ratio distribution might be affected by selection effects is not yet clear.

What is clear, however, is that the mass ratios of binaries with primary masses greater than $0.5\,M_\odot$ do not agree with Duquennoy & Mayor's mass ratio distribution. Of the 34 binaries, only 10 have mass ratios less than $M_2/M_1 = 0.5$.

In Fig. 20, we display the stellar (primary masses $>0.1\,M_\odot$) and VLM mass ratio distributions from the rerun calculation (lower panels) and the main calculation at the same time ($t = 1.038t_{\rm ff}$; upper panels). The stellar mass ratio distributions are not significantly different from each other or from Fig. 19. However, the VLM binary mass ratio distributions at early times (for both the main and rerun calculations) are flatter than that obtained at the end of the main calculation. *Again, this implies that the properties of the VLM binaries evolve.* Both the apparent evolution of VLM binary separations and mass ratios are consistent with the evolution discussed by Bate et al. (2002b). Dynamical exchange interactions between binaries
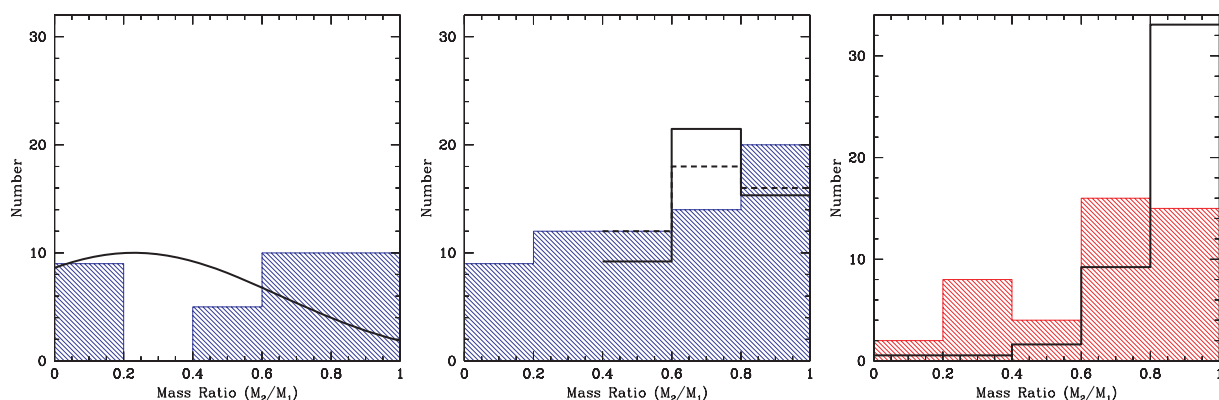

Figure 19. The mass ratio distributions of binary systems with stellar primaries in the mass ranges $M_1 > 0.5\,M_\odot$ (left-hand panel) and $M_1 = 0.1$–$0.5\,M_\odot$ (centre) and VLM primaries (right-hand panel; $M_1 < 0.1\,M_\odot$) produced by the main calculation. The solid black lines give the observed mass ratio distributions of Duquennoy & Mayor (1991) for G dwarfs (left-hand panel), Fischer & Marcy (1992) for $M_1 = 0.3$–$0.57\,M_\odot$ (centre, solid line) and $M_1 = 0.2$–$0.57\,M_\odot$ (centre, dashed line) and of the known VLM binary systems maintained by Nick Siegler at http://vlmbinaries.org/ (right-hand panel). The observed mass ratio distributions have been scaled so that the areas under the distributions ($M_2/M_1 = 0.4$–1.0 only for the centre panel) match those from the simulation results. The VLM binaries produced by the simulation are biased towards equal masses when compared with M-dwarf binaries (primary masses in the range $M_1 = 0.1$–$0.5\,M_\odot$). 71 per cent of the VLM binaries have $M_2/M_1 > 0.6$ while for the M-dwarf binaries the fraction is only 51 per cent.
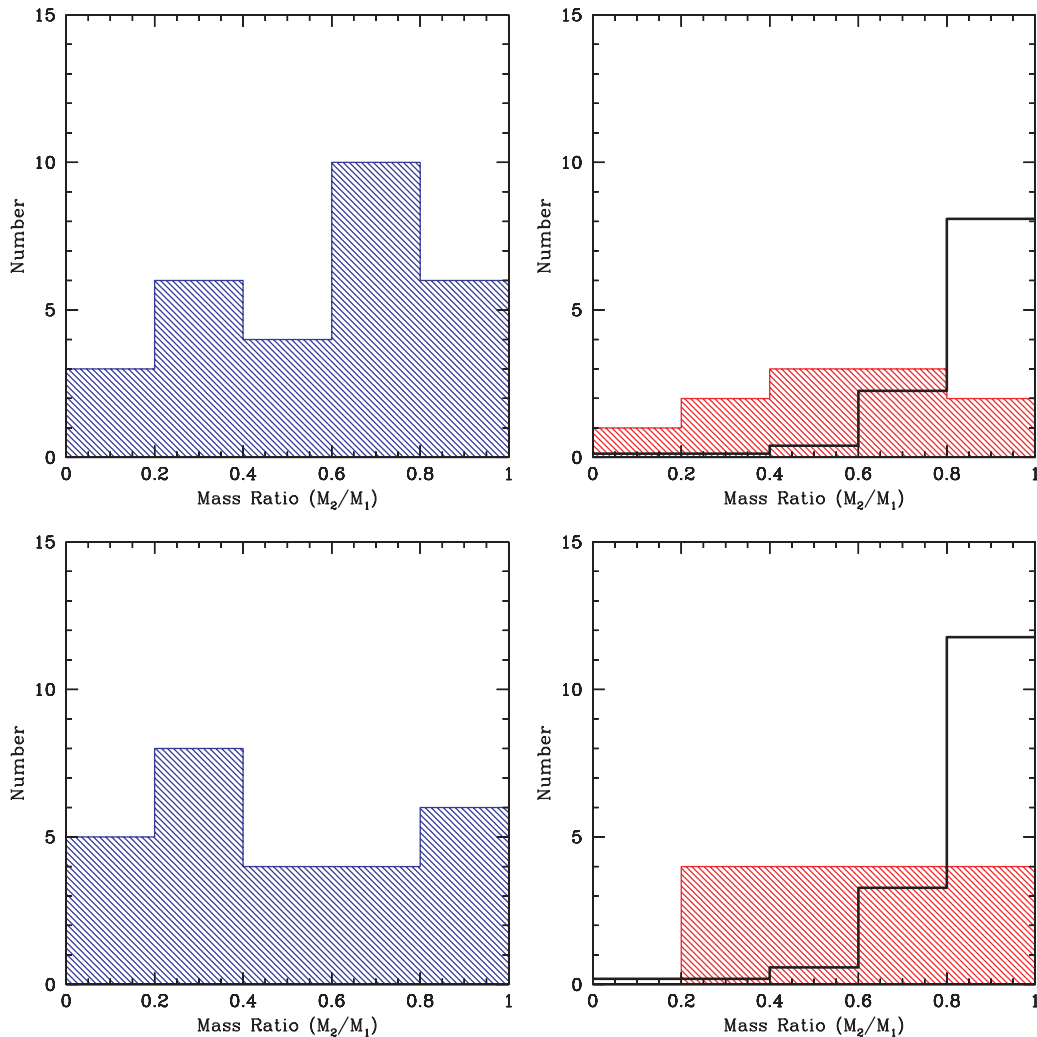
Figure 20. The mass ratio distributions of binary systems with stellar ($M_1 > 0.1\,\mathrm{M}_\odot$; left-hand panels) and VLM (right-hand panels) primaries produced by the main calculation (upper panels) and rerun calculation (lower panels), both at $t = 1.038 t_{\mathrm{ff}}$. In the VLM graphs, the open black histogram gives the mass ratio distribution of the known VLM multiple systems maintained by Nick Siegler at http://vlmbinaries.org/ (scaled to match the total number) . The frequency of VLM binaries is higher in the rerun calculation, but the mass ratio distributions of both stars and VLM objects are indistinguishable given the small number statistics. Comparing the VLM panels with that in Fig. 19, there is evidence that the VLM binaries begin with more uniform mass ratio distributions and evolve towards equal masses as the main calculation proceeds.

and single objects tend to produce more equal-mass components, as does accretion of gas from circumbinary discs or the accretion of infalling gas with high specific angular momentum. Thus, the apparent evolution of both the VLM binary separations and mass ratios may be due to evolution during their formation.

3.6.1 Mass ratio versus separation

In Fig. 21, we plot mass ratios against separation (semimajor axis) for the binaries, triples and quadruples at the end of the main calculation. Note that for this figure we include systems that are subcomponents of higher-order systems. Thus, the closest two objects in a triple also appear in the plot as a binary. Similarly, for quadruples consisting of two binary subcomponents, each of the binaries appears in the plot and for each of the quadruples that involves a triple system, the triple appears in the plot.

There is clearly a relation between mass ratio and separation for the binaries with closer systems having a preference for equal masses. The median mass ratios for *binary* separations in the ranges

1–10, 10–100, 100–1000 and 1000–10^4 au are $M_2/M_1 = 0.74, 0.57,$ 0.68 and 0.17, respectively. Including the mass ratios of triples and quadruples (as defined in the caption of Fig. 21), these median values become 0.74, 0.41, 0.15 and 0.07, respectively. The median mass ratio for triples is 0.11 and for quadruples is 0.07. However, the quadruples include those composed of two binaries and those composed of a triple and a fourth wide component. The mass ratios of the latter tend to be much lower than those of the former. There are eight quadruples composed of two binaries and 16 composed of triples and a fourth component. The median mass ratios for these two subsamples are 0.45 and 0.03, respectively. There are also only 11 (out of 40) triples composed only of stars (as opposed to containing VLM objects). For these, the median mass ratio is 0.48. All but one of the quadruple systems contain at least one VLM object.

A trend of more unequal-mass binaries with increasing separation is expected from the evolution of protobinary systems accreting gas from an envelope (Bate 2000). Furthermore, dynamical interactions between binaries and single stars tend to tighten binaries at the
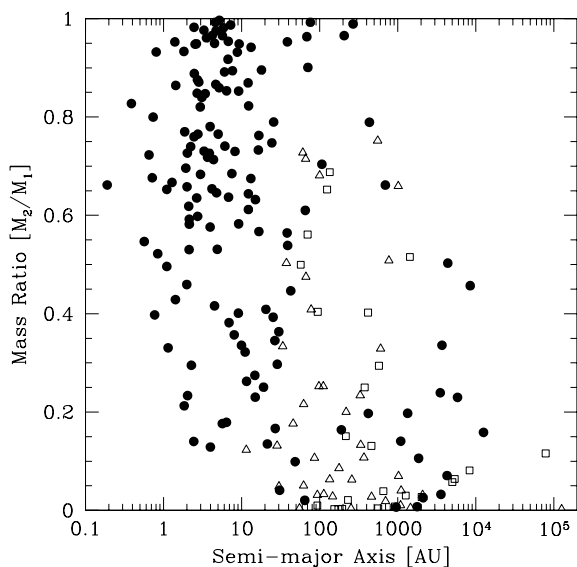
Figure 21. The mass ratios of binaries (filled circles), triples (open triangles) and quadruples (open squares) as a function of semimajor axis for the main calculation. For triples, the mass ratio compares the mass of the widest component to the sum of the masses of the two closest components. For quadruples involving a two binary components, the mass ratio is between the two binaries, and for quadruples involving a triple, the mass ratio is between the mass of the fourth component and the triple. All mass ratios are defined to be ≤ 1. There is a clear relationship between mass ratio and separation with closer binaries having a greater fraction of near equal-mass systems.

same time as increasing the binary mass ratio through exchange interactions.

Observationally, closer binaries are found to have a higher fraction of 'twins' (Soderhjelm 1997; Tokovinin 2000b; Halbwachs et al. 2003). Tokovinin (2000b) found evidence for the frequency of twins falling off for orbital periods greater than 40 d, but Halbwachs et al. (2003) found that the fraction of near equal-mass systems ($M_2/M_1 > 0.8$) is always larger for shorter period binaries than longer period binaries regardless of the dividing value of the period (from just a few days up to 10 yr). However, despite the fact that the fraction of twins decreases with increasing separation, the mass ratio distributions of both the short- and long-period binaries appear to have a peak at $M_2/M_1 = 1$ (e.g. Tokovinin 2000b; Halbwachs et al. 2003; Söderhjelm 2007). These observed relations are in qualitative agreement with the decreasing median mass ratio with increasing separation discussed above. In Fig. 21, we also note that although there is a higher fraction of twins at small separations, there are still some wide twins (separations 30–300 au).

For stellar triple and quadruple systems, Tokovinin (2008) reports that triples are observed to have a median mass ratio of 0.39 independent of the outer orbital period, while quadruples involving two binary subcomponents have a similar median mass ratio of ≈ 0.45, but there may be a dependence on the outer orbital period. The median mass ratio of the triple systems from the main calculation is in agreement with the observations, as long as we only consider the triples containing stellar components (no VLM components). This is consistent with the observational sample, but it does raise the question of how many triple systems containing VLM components exist in reality. Similarly, the median mass ratio of quadruples containing two binary subsystems is in good agreement with observations, but all but one of the systems from the

main calculation include a VLM object, whereas the observational sample is dominated by stellar-only systems. It is also interesting to note that quadruples composed of a triple and a wide fourth component outnumber quadruples composed of two binaries by 2:1 in the main calculation. Tokovinin (2000a) finds roughly equal numbers of such quadruples. However, if the wide components of quadruples containing triples as subcomponents typically have low masses, this could be attributed to observational bias.

For the binaries, the clear trend of decreasing mass ratio with separation may go some way to explain the apparent deficit of unequal-mass binaries with primary masses greater than 0.5 $M_\odot$ in the main calculation (left-hand panel of Fig. 19). It is clear from Figs 17 and 21 that the main calculation does not produce many wide pure binaries – most of the wide systems are triples or quadruples, and the binary components within them necessarily have smaller separations than the wide tertiary or quartic components. Since the mass ratio distributions in Fig. 19 only contain binary mass ratios an unequal-mass visual binary may in fact be composed of an undetected close binary and a wider companion. However, while an observer of the system would include the unequal-mass ratio of the wide system, only the mass ratio of the close binary component would be included in a mass ratio distribution like Fig. 19.

Therefore, one way to reconcile the main calculation with observations may be to include the mass ratios of tertiary and quartic components. The problem with this is that there is no unique way to do this – should the mass ratio of a triple be simply the ratio of the total mass of the binary to the third component? Should an attempt be made to model the luminosities of the two stars in the binary? What if the ratio of the two separations is small so that if an observer identified it as a binary, they would also have been likely to separate it into a triple? Furthermore, Duquennoy & Mayor (1991) actually found a rather low frequency of triple and higher-order systems anyway, so perhaps the question of how to treat these higher-order systems is not important. On the other hand, discussion continues as to how many triples and quadruples were missed by this and other surveys.

For the moment, we conclude that the main calculation appears to underproduce unequal-mass solar-type binaries compared with observations. However, this may at least be partially reconciled if many of the observed binaries are in fact higher-order systems or, alternately, if the mass ratios of tertiary and quartic components from the main calculation are included in the statistics. There is much less of a difference between observations and the main calculation for binaries with M-dwarf primaries or VLM binaries simply because (a) the frequency of higher-order systems decreases rapidly with decreasing primary mass (Section 3.4.3), so the issue of how to treat higher-order systems does not arise and (b) the typical separation of binaries decreases with decreasing primary mass (Section 3.5), so the wider systems that tend to have more unequal masses are much less frequent for low primary masses.

3.7 Orbital eccentricities

Observationally, there is observed to be an upper envelope to binary eccentricities at periods less than a few years (Duquennoy & Mayor 1991; Halbwachs et al. 2003). However, the main calculation does not allow us to probe such small separations. Observations also indicate that eccentricities $e < 0.1$ are rare for periods greater than ≈ 100 d (separations $\gtrsim 1$ au). Finally, Halbwachs et al. (2003) find that the eccentricities of so-called 'twins' (binaries with mass ratios $M_2/M_1 > 0.8$) with periods greater than ≈ 10 d (the tidal

circularisation radius) are lower than for more extreme mass ratio systems.

In the upper panel of Fig. 22, we plot the eccentricities versus semimajor axes of the orbits of the binaries, triples and quadruples from the main calculation. The distribution of eccentricities looks reasonable for separations greater than 10 au. In particular, of the 122 orbits with separations greater than 10 au, there are only seven orbits with $e < 0.1$, and all these have separations between 10 and 100 au.

However, there appears to be a strong excess of systems with $e > 0.7$ and separations less than 10 au. This is almost certainly an artefact introduced by the sink particle approximation. The absence of gas closer than 5 au from a sink particle means that the dissipative interactions between binary stars and the gas orbiting them are absent. In Fig. 22, we also plot eccentricity versus semimajor axis for the orbits of binaries, triples and quadruples from the main calculation (middle panel) and rerun calculation (lower panel) at $t = 1.038t_{ff}$. The rerun calculation has no indication of the excess population at separations less than 10 au and $e > 0.7$, whereas even at this early time the main calculation has five binaries with separations less than 10 au and $e > 0.8$. Thus, as expected, reducing the sink particle accretion radii allows dissipative interactions between sink particles on smaller scales and brings the calculations into better agreement with the observed eccentricity distributions. The mean eccentricity of the systems in the rerun calculation is $\langle e \rangle = 0.44$ for the binaries only, and $\langle e \rangle = 0.45$ if the orbits of the triples and quadruples are also taken into account. The mean binary eccentricity is in good agreement with the observed mean eccentricities of long-period binaries (periods $P \gtrsim 300$ d; Duquennoy & Mayor 1991; Halbwachs et al. 2003).

We have also examined the dependence of the eccentricity on the mass ratio (for binary orbits only, but including binaries that are also components of higher-order system) to see whether there is any sign of the tentative correlation between mass ratio and eccentricity found by Halbwachs et al. (2003). For the main calculation, the median eccentricity of binaries with mass ratios $M_2/M_1 < 0.8$ is $e = 0.74$ (100 orbits), while for $M_2/M_1 > 0.8$, the median is $e = 0.55$ (46 orbits). Excluding orbits with separations less 10 au (since they likely have high eccentricities due to the absence of dissipation on small scales), the median eccentricity of binaries with mass ratios $M_2/M_1 < 0.8$ is $e = 0.47$ (47 orbits), while for $M_2/M_1 > 0.8$, the median is $e = 0.37$ (10 orbits). For $M_2/M_1 > 0.9$, the median is only $e = 0.34$ (seven orbits). For the rerun calculation, the statistics are that the median binary eccentricity for mass ratios $M_2/M_1 < 0.8$ is $e = 0.45$ (33 orbits), while for $M_2/M_1 > 0.8$, the median is $e = 0.39$ (10 orbits) and $e = 0.36$ for $M_2/M_1 > 0.9$ (only five orbits). Thus, in all cases, *we find evidence for a link between mass ratio and eccentricity such that 'twins' have lower eccentricities, as is observed, though the effect is quite weak.*

3.8 Relative alignment of orbital planes for triples

For a hierarchical triple system there are two orbital planes, one corresponding to the short-period orbit and one to the long-period orbit. There are many reasons why the inclinations of the orbital planes may not be randomly distributed relative to one another. For example, if the triple system forms from the fragmentation of a disc around an initially single object, the orbital planes would be expected to be nearly coplanar. If a triple system forms from a flatten core, it may have preferentially aligned orbital planes. If a triple system forms with initially non-coplanar orbital planes and
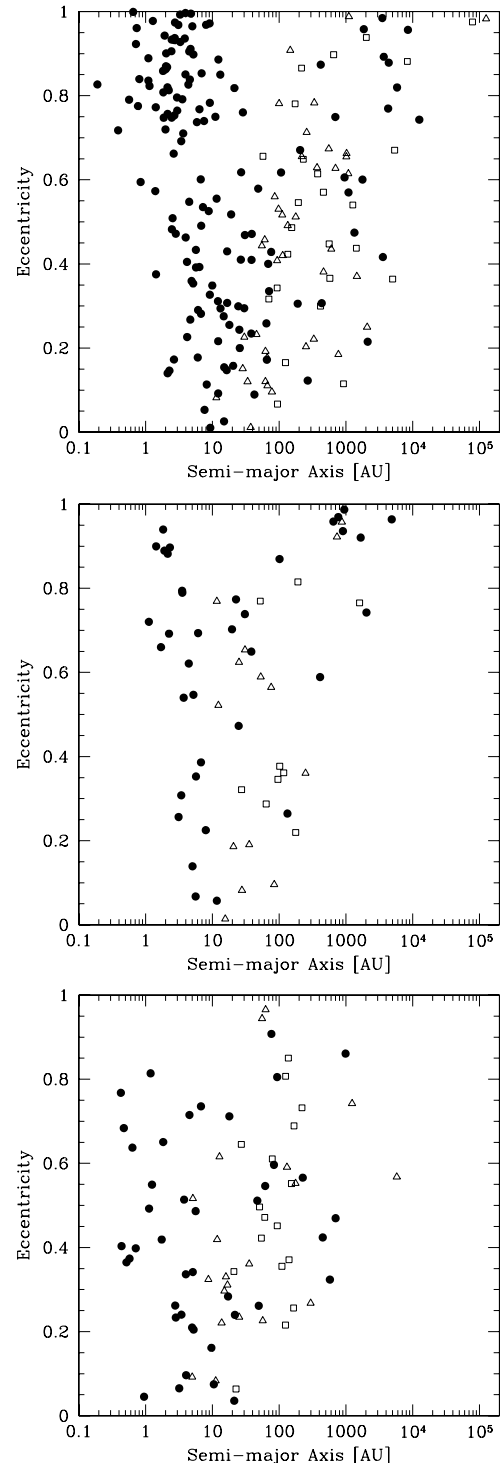

Figure 22. The eccentricity distribution of binary (filled circles), triple (open triangles) and quadruple orbits (open squares) as a function of semi-major axis for the main calculation at the end (top panel) and at $t = 1.038t_{ff}$ (centre) and for the rerun calculation (lower panel). The distribution at the end of the main calculation looks reasonable except for the group of binaries with semimajor axes less than $\sim$10 au and eccentricities $e \gtrsim 0.7$. These systems would presumably have smaller eccentricities if the gas dynamics inside 5 au of each sink particle were modelled. This is tested by comparing the main calculation with the rerun calculation at $t = 1.038t_{ff}$ (the lower two panels). As expected, although the main calculation still has a group of highly eccentric close binaries, these systems are absent in the rerun calculation.

subsequently accretes a lot of mass, this may drive its orbital planes into closer alignment. On the other hand, if a triple system forms from capture of a single object by a binary, the orbital planes may be very misaligned. Similarly, the wide tertiary in an initially aligned triple system may be perturbed by a passing object resulting in misaligned orbits.

Observationally, it is difficult to determine the relative orientations of the two orbits of a triple system due to the number of quantities that must be measured to fully characterize the orbits. In particular, the relative angle between the two orbital angular momentum vectors is given by

$$\cos \Phi = \cos i_1 \cos i_2 + \sin i_1 \sin i_2 \cos(\Omega_1 - \Omega_2), \qquad (3)$$

where i_1 and i_2 are the orbital inclinations and Ω_1 and Ω_2 are the position angles of the lines of nodes. The latter are only known with $180°$ ambiguity unless the ascending node is identified by radial velocities. Because for most observed triple systems the sign of the $\cos(\Omega_1 - \Omega_2)$ term is not known, there are two possible values of Φ. On the other hand, the mean value of Φ can be measured simply from the knowledge of the number of corotating and counter-rotating systems (Worley 1967; Tokovinin 1993; Sterzik & Tokovinin 2002). These facts are important when we come to compare our results with observations below.

The first studies (Worley 1967; van Albada 1968) of the relative orbital orientations of triple systems found a small tendency towards alignment of the angular momentum vectors of the orbits. Of 54 systems with known directions of the relative motions, 39 showed corevolution and 15 counter-revolution resulting in a mean relative inclination angle of $\langle \Phi \rangle \approx 50°$. For 10 visual systems with known orbits, five systems were found to have $\Phi < 90°$, two had $\Phi > 90°$ and three were ambiguous. Fekel (1981) examined 20 systems with known orbits and periods of less than 100 yr (for the wide orbit). He found that one-third had non-coplanar orbits. Finally, Sterzik & Tokovinin (2002) performed the most detailed study to date. From 135 visual triple systems for which the relative directions of the orbital motions are known, they found $\langle \phi \rangle = 67° \pm 9°$, and this result was also consistent with 22 systems for which the orbits were known. They also found a tendency for the mean relative orbital angular momentum angle to increase with increasing orbital period ratio (i.e. systems with more similar orbital periods tend to be more closely aligned).

At the end of the main calculation, there are 40 triple systems (17 of these are subcomponents of quadruple systems). The mean relative orientation angle of these systems is $\langle \Phi \rangle = 65° \pm 6°$, in very good agreement with the observed value mentioned above. This indicates that both the observed and simulated triple systems have a small tendency towards orbital coplanarity. The rerun and the main calculations at $t = 1.038 t_{\mathrm{ff}}$ formed 20 and 14 triples with $\langle \Phi \rangle = 53° \pm 7°$ and $69° \pm 13°$, respectively. In Fig. 23, we compare the cumulative distributions of the orbital orientation angles for the triple systems of Sterzik & Tokovinin (2002) with those formed by the main calculation at the end and at $t = 1.038 t_{\mathrm{ff}}$, and by the rerun calculation. The observational results (solid lines) include two angles for each observed triple system due to the ambiguity described above. For the simulation results, we plot two cumulative distributions, one with the actual angles (dot–dashed lines) and one with two angles (dashed lines) for each triple (the true angle and the other possible angle allowed by reversing the rotation of one of the orbits). *The observed and simulated distributions are in good agreement* when the angle ambiguity is included, but even without including the angle ambiguity, the simulations are consistent with the observations.
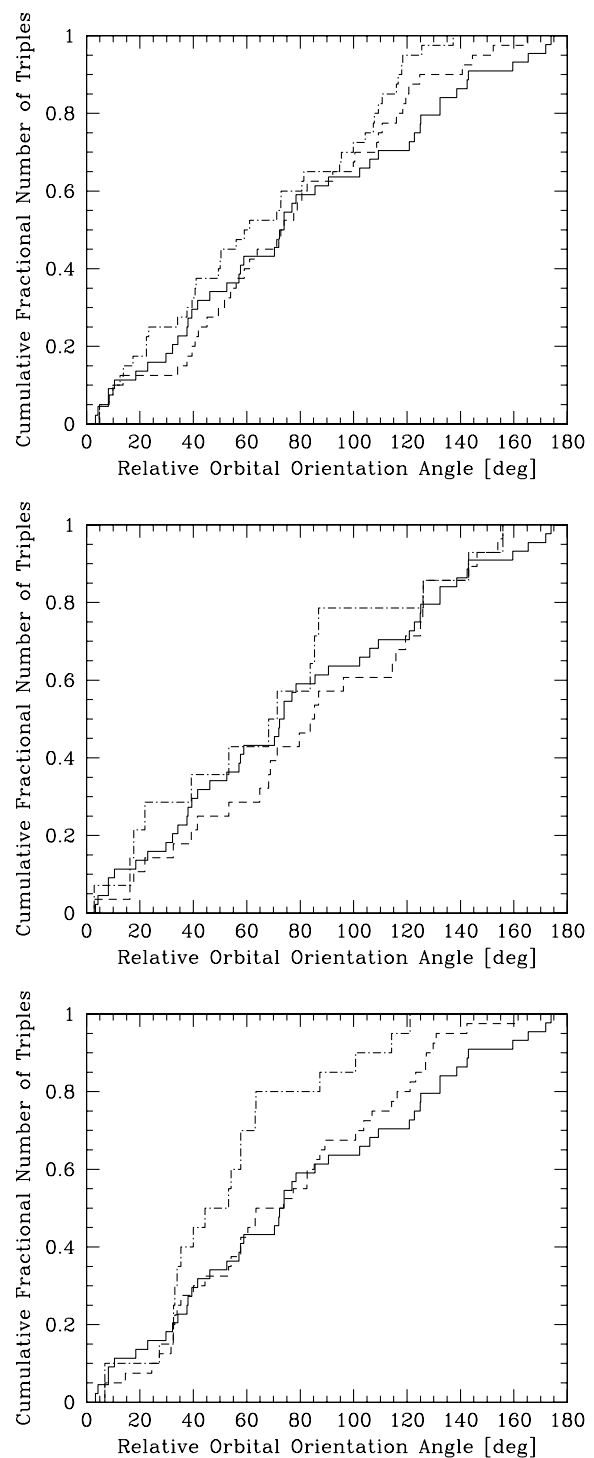

Figure 23. The cumulative fraction of triples as a function of their relative orbital orientation angles at the end of the main calculation (top panel) and at $t = 1.038 t_{\mathrm{ff}}$ for the main calculation (centre) and the rerun calculation (bottom panel). In each case, the solid line gives the observed distribution of orientation angles including the $\cos(\Omega_1 - \Omega_2)$ ambiguity (Sterzik & Tokovinin 2002), the dot–dashed line gives the actual result from the simulation, and the dashed line gives the simulation result including the ambiguity present in the observed values. All simulated distributions are consistent with the observed distribution. When the simulated distributions include the angle ambiguity, the probabilities that they are drawn from the same population as the observed systems are 54, 72 and 66 per cent, respectively. Even when the actual simulated distributions are compared with the observed distribution the probabilities are 14, 88 and 3.5 per cent, respectively.
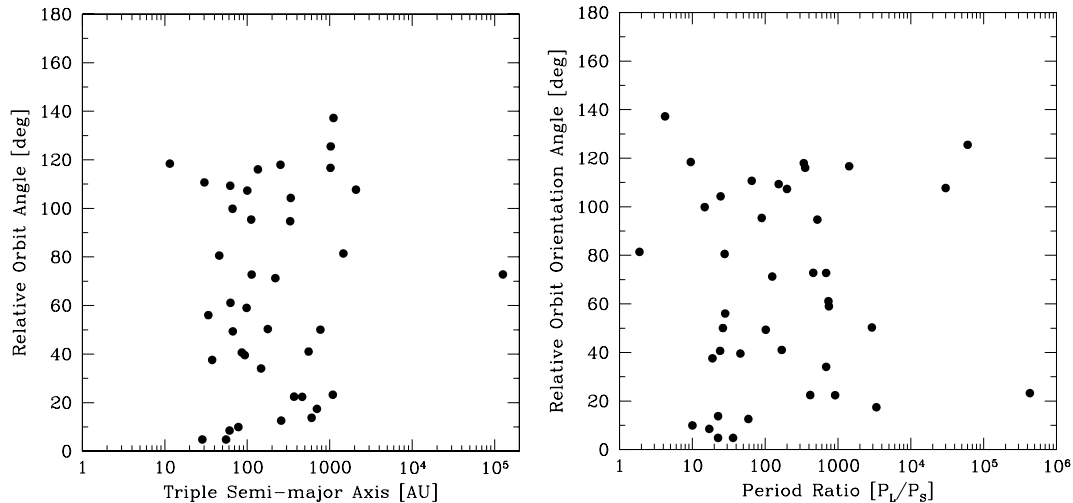
Figure 24. The relative inclinations of the two orbital planes for the 40 triple systems produced by the main calculation (including those that are subcomponents of quadruples). We give plots of the relative orbital orientation angle versus the semimajor axis of the third component (left) and versus the period ratio of the long and short-period orbits (right). There are no triples with relative orbital angles $>140°$. There is also the hint of an excess of systems with relative orbital angles less than $\approx 20°$ for systems with period ratios less than 100. Note that the two systems with period ratios $P_{\rm L}/P_{\rm S} < 5$ are still dynamically unstable and would certainly undergo further evolution.

In Fig. 24, we plot the relative orbital orientation angle of the 40 triple systems as functions of the semimajor axis of the wide orbit and the ratio of the two orbital periods. There is no clear correlation between the orbital orientation angle and the semimajor axis or period ratio, or indeed on other quantities such as primary mass or the eccentricity of the long-period orbit. However, although the triples are formed with a wide range of relative orbital inclinations, the absence of any angle greater than $140°$ seems to be significant. This implies that the triple systems are not formed purely by the capture of a third component. We also note that there appears to be a small collection of four nearly coplanar triples with wide semimajor axes less than 100 au, or six nearly coplanar triples with period ratios of less than 100. This is intriguing, but unfortunately not statistically significant.

As mentioned above, Sterzik & Tokovinin (2002) found a tendency for the mean relative orbital orientation angle to increase with increasing period ratio. In Fig. 25, we reproduce their observed results and plot our results from the main and the re-run calculations. Here, we have performed averages over four groups of 10 (five for the rerun calculation) triples, sorted by period ratio. Our results are consistent with the observed values and there may be a hint of a dependency on the period ratio, but our results are also consistent with no dependence. Better statistics are required for both the simulations and observations to validate this trend.

Figure 25. The mean relative orbital orientation angle for triple systems. The blue filled circles give the results at the end of the main calculation with their statistical uncertainties. The red open circles give the results from the rerun calculation. The main calculation has not formed enough triple systems at $t = 1.038t_{\rm ff}$ to enable meaningful data to be plotted at the earlier time. The black crosses give the observed mean angles from the Mulitple Star Catalogue as calculated by Sterzik & Tokovinin (2002). The calculations are consistent with the observations and hint at an increasing mean orientation angle with increasing period ratio, but they are also consistent with a mean orientation angle that is independent of the period ratio.

3.9 Relative alignment of discs and orbits

Finally, we consider the relative alignment of the spins of the sink particles in binary systems. Unfortunately, there is not a direct analogy with real binary systems in this case because the sink particles are larger than stars and yet smaller than a typical disc. The orientation of the sink particle spin thus represents the orientation of the total angular momentum of the star and the inner part of its surrounding disc. This distinction is important because during the formation of an object the angular momentum usually varies with time as gas falls on to it from the turbulent cloud. Thus, the orientation of the sink particle frequently differs substantially from the
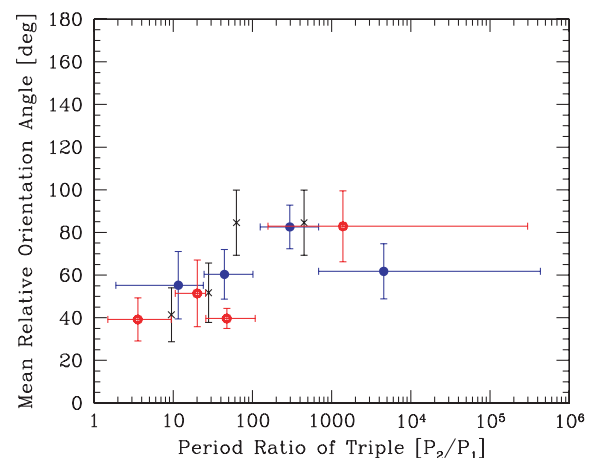
orientation of its resolved disc (if one exists) and, furthermore, the orientations of both the sink particles and their discs change with time while the object continues to accrete gas.

Observationally, Weis (1974) found a tendency for alignment between the stellar equatorial and orbital planes among primaries in F-star binaries, but not A-star binaries. The orbital separations were mainly in the 10–100 au range. Similarly, Guthrie (1985) found no correlation for 23 A-star binaries with separations 10–70 au. Most recently, Hale (1994) considered 73 binary and multiple systems containing solar-type stars and found evidence for approximate coplanarity between the orbital and the stellar equatorial planes for

binary systems with separations less than ≈ 30 au and apparently uncorrelated stellar rotation and orbital axes for wider systems. For higher-order multiple systems, however, non-coplanar systems were found to exist for both wide and close orbits. Hale found no evidence to support a difference dependent on spectral type, eccentricity or age. In terms of circumstellar discs, there is evidence for misaligned discs from observations of misaligned jets from protostellar objects (Davis, Mundt & Eisloeffel 1994), inferred jet precession (Eisloffel et al. 1996; Davis et al. 1997) and direct observations (Koresko 1998; Stapelfeldt et al. 1998). However, these are not statistically useful samples. Finally, Monin, Menard & Duchene (1998), Jensen et al. (2004), Wolf, Stecklum & Henning (2001) and Monin, Ménard & Peretto (2006) used polarimetry to study the relative disc alignment in T-Tauri wide binary and multiple systems. They all found a preference for disc alignment for binaries. However, Jensen et al. (2004) also found that the wide components of triples and quadruples appear to have random orientations.

For the main calculation (either at the end or at $t = 1.038 t_{ff}$), we find no significant dependence of the relative orientation of the two sink particle spins on mass ratio, semimajor axis, period or eccentricity. The relative orientations appear to be random. We do not explicitly consider the relative orientation of the sink particle spins and the orbital plane since if the sink particle spins are uncorrelated with each other, then by definition they cannot (both) be closely correlated with the orbital axis. The mean relative orientation angle for the 146 binaries (including those that are components of triple and quadruple systems) is $88° \pm 3°$ at the end of the main calculation and $79° \pm 7°$ at $t = 1.038 t_{ff}$ (37 binaries). For the rerun calculation, with smaller accretion radii and orbital periods, the mean angle is $73° \pm 7°$ (43 binaries) and there is a hint that short-period binaries (periods less than a few years) may have preferentially aligned spins but it is not statistically significant (see Fig. 26). For all of the calculations, there is also a hint that the most massive binaries have preferentially aligned spins, but only for the rerun calculation is the reduction in the mean relative angle statistically significant. In this case, the mean angle for most massive quartile of binaries (11 out of 43, having total binary masses greater than $\approx 0.6\,M_\odot$) is $38° \pm 12°$ which differs from a random value of $90°$ by more than 4σ, while the mean angle for the other three quartiles is each within

0.5σ of $90°$ (see the left-hand panel of Fig. 26). Within the competitive accretion paradigm, the reason that the most massive binaries tend to have aligned rotation axes is presumably that they have both accreted a lot of gas from a common reservoir in order to become massive binaries and that any initial variation in their rotation axes has been decreased by the long period of accretion. The components of less massive binaries, on the other hand, still largely retain their initial (randomly orientated) rotation axes. Unfortunately, the observational surveys mentioned above are somewhat ambiguous on whether or not there is a dependence of alignment of the stellar rotation axes on the total binary mass.

4 CONCLUSIONS

We have presented results from the largest hydrodynamical simulation of star cluster formation to date that resolves the opacity limit for fragmentation. It also resolves protoplanetary discs (radii ≥ 10 au) and binaries with separations as small as 1 au. The calculation produced 1254 stars and brown dwarfs. This large number of objects allows detailed comparison of the statistical properties of the stars, brown dwarfs and multiple systems with the results of observational surveys. We also reran part of the simulation with smaller sink particles and no gravitational softening between sink particles allowing discs with radii ≥ 1 au to be resolved and binaries as close as 0.02 au to test the dependence of the results on the sink particle approximation. Our conclusions are as follows.

(i) The calculations produce an IMF with a similar form to the observed IMF, including a Salpeter-type slope at the high-mass end, but they overproduce brown dwarfs. The brown dwarf to star ratio is 3:2 from the main calculation, whereas observationally it is estimated to be more like 1:3. This does not appear to be a result of using sink particles. Rather, it is likely due to the absence of radiative feedback and/or magnetic fields in the calculations.

(ii) As in previous, smaller calculations, the IMF originates from competition between accretion and ejection, which terminates the accretion and sets an object's final mass. Stars and brown dwarfs form in the same way, with similar accretion rates from the
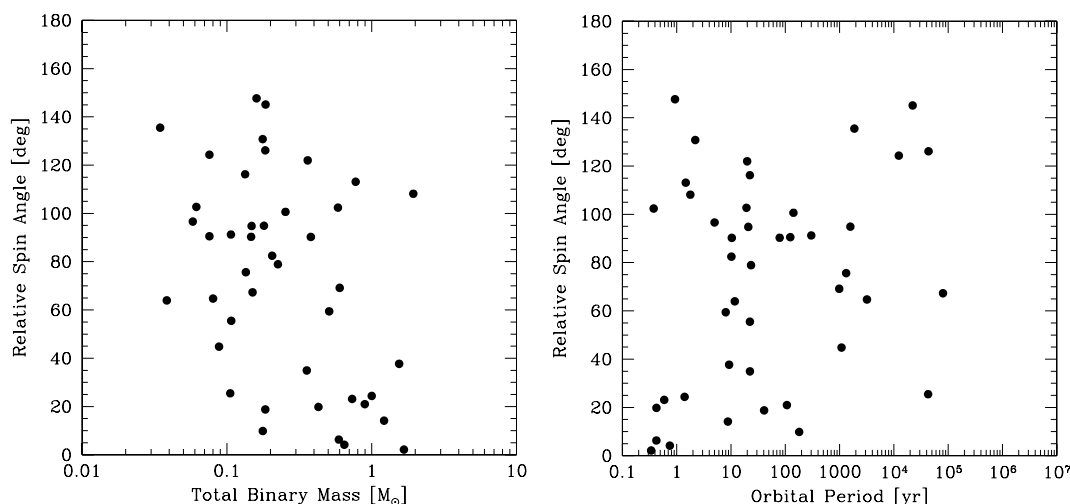
Figure 26. The relative inclinations of the rotation axes of the sink particles (modelling stars and their inner discs) of the binary systems produced by the rerun calculation (including those that are subcomponents of triples and quadruples). There is an excess of nearly aligned systems with a high total mass and/or orbital periods less than a few years. The main calculation also shows a slight tendency for high-mass binaries to have aligned rotation axes, but it is not statistically significant (see the main text).

molecular cloud, but stars accrete for longer than brown dwarfs before undergoing the dynamical interactions that terminate their accretion.

(iii) We examine the dependence of binarity, velocity dispersion and the IMF on the distance from the centre of the resulting stellar cluster. We find that the binarity and velocity dispersion are constant throughout the bulk of the cluster, but beyond three half-mass radii (the outer 20 per cent of the stellar mass), the binarity decreases and the velocity dispersion increases because these objects have been ejected. We find that stars have a slightly higher velocity dispersion than VLM objects, and binaries have a significantly lower velocity dispersion than single objects. Contrary to the expectations of competitive accretion, we find no evidence of mass segregation. This may be because the stellar cluster was formed from the merger of five subclusters shortly before the calculation was stopped.

(iv) We examine the potential effect of dynamical interactions on protoplanetary disc sizes. We find that the typical truncation radius decreases with increasing stellar mass (i.e. more massive stars have had closer encounters). It is difficult to directly associate the closest encounter with the radii of protostellar discs because many stars accrete new discs after suffering a close encounter. This is particularly true for the more massive stars. However, for VLM objects, dynamical encounters usually occur soon after their formation and terminate their accretion so their truncation radii may more closely reflect their disc radii. Under this assumption, we find that at least 10 per cent of the VLM objects should have disc radii >40 au. In lower density star-forming environments, this fraction may be expected to be larger. More massive stars that undergo close encounters and do not subsequently accrete new discs may be the source of WTTS with very young ages ($\lesssim 1$ Myr).

(v) We find that multiplicity strongly increases with primary mass. The results from the main calculation are in good agreement with the observed multiplicities of G, K and M dwarfs. For VLM objects with primary masses 0.03–0.10 $M_\odot$, the multiplicity fraction is 0.10 ± 0.03 which is lower than the observations by a factor of 2. However, when smaller accretion radii are used the VLM multiplicity rises to 0.19 ± 0.05, in good agreement with observations. Therefore, we conclude that hydrodynamical simulations are able to match the observed multiplicities if the resolution is adequate. We also predict that the multiplicity continues to drop below 30 Jupiter masses. We expect a multiplicity no more than ≈ 7 per cent for objects with masses 10–30 Jupiter masses, and less than 3 per cent for primaries of less than 10 Jupiter masses.

(vi) We find very low frequencies of VLM companions to stars, and we find that the frequency does not depend strongly on primary mass. However, the median star–VLM separation strongly increases as primary mass increases from less than 10 au for 0.1–0.2 $M_\odot$ primaries to ~ 50 au for masses $\approx 0.4 M_\odot$ and >100 au for solar-type stars.

(vii) We examine the separation distributions of binaries, triples and quadruples. We find that the median separation decreases with decreasing primary mass with stellar systems having a median separation of ≈ 26 au and VLM systems ≈ 10 au. This trend is in agreement with observed systems, but is not as strong. At small separations, the distributions are dependent on the sink particle parameters. Better agreement is obtained with smaller sink particle accretion radii and gravitational softening.

(viii) The mass ratio distribution of M-dwarf binaries is roughly flat and consistent with observations. VLM systems have a strong preference for equal masses, but not as strong as it appears to be the case for observed systems. However, for K- and G-type primaries, the calculations underproduce unequal-mass systems. We

find that closer binaries tend to have a higher proportion of equal-mass components in broad agreement with observed trends. We also find reasonable agreement with observations on the mass ratios of triples and quadruples, but with relatively large uncertainties from both the simulation and observations.

(ix) We find that the separations and mass ratios of VLM binaries evolve during their formation from wide systems with unequal masses towards close, equal-mass systems.

(x) The main calculation produces a strong excess of short-period highly eccentric binaries. However, when smaller sink particle accretion radii and gravitational softening are used, this excess disappears leaving a reasonable eccentricity distribution with a mean eccentricity that is in agreement with observations. We also find a weak link between mass ratio and eccentricity such that 'twins' have lower eccentricities, as is observed.

(xi) We investigate the relative orientation of the orbital planes of triple systems. We obtain a mean orientation angle of $\langle \Phi \rangle = 65° \pm 6°$ from the main calculation in excellent agreement with the observed value. Thus, triples have a small tendency for orbital alignment. The distribution of orientation angles is also in agreement with observations. There is an absence of relative angles greater than $\approx 140°$ in the simulated triples.

(xii) Finally, we study the relative orientations of sink particle angular momentum vectors in binaries (analogous to the rotation axes of stars and their inner discs). We find no significant tendency towards alignment. However, there is weak evidence that the most massive binaries and/or the shorter period systems may have a tendency for alignment. Observations suggest that shorter period binaries have a tendency towards alignment.

Overall, the hydrodynamical star cluster formation simulations display good agreement with a wide range of the observed statistical properties of stellar systems. There are only two areas of poor agreement: the overproduction of brown dwarfs relative to stars and the lack of unequal-mass K- and G-dwarf binaries. The former of these is likely due to the absence of radiative feedback and/or magnetic fields in the simulations, but the reason for the latter is unclear.

Finally, we note that from this point forward, numerical simulations of star formation should be capable of producing precise predictions for the statistical properties stars. The precision of observational surveys will soon become the limiting factor in comparing the results of numerical simulations with observations. The results of large observational surveys of stellar properties will be needed in the near future.

REFERENCES

Ahmic M., Jayawardhana R., Brandeker A., Scholz A., van Kerkwijk M. H., Delgado-Donate E., Froebrich D., 2007, ApJ, 671, 2074

Allen P. R., Koerner D. W., McElwain M. W., Cruz K. L., Reid I. N., 2007, AJ, 133, 971

Andersen M., Meyer M. R., Greissl J., Aversa A., 2008, ApJ, 683, L183

Armitage P. J., Clarke C. J., 1997, MNRAS, 285, 540

Armitage P. J., Clarke C. J., Palla F., 2003, MNRAS, 342, 1139

Basri G., Reiners A., 2006, AJ, 132, 663

Bate M. R., 2000, MNRAS, 314, 33

Bate M. R., 2005, MNRAS, 363, 363 (B2005)

Bate M. R., Bonnell I. A., 2005, MNRAS, 356, 1201

Bate M. R., Burkert A., 1997, MNRAS, 288, 1060

Bate M. R., Bonnell I. A., Price N. M., 1995, MNRAS, 277, 362 (BB2005)

Bate M. R., Clarke C. J., McCaughrean M. J., 1998, MNRAS, 297, 1163

Bate M. R., Bonnell I. A., Bromm V., 2002a, MNRAS, 332, L65

Bate M. R., Bonnell I. A., Bromm V., 2002b, MNRAS, 336, 705

Bate M. R., Bonnell I. A., Bromm V., 2003, MNRAS, 339, 577 (BBB2003)

Benz W., 1990, in Buchler J. R., ed., Numerical Modelling of Nonlinear Stellar Pulsations Problems and Prospects. Kluwer, Dordrecht, p. 269

Benz W., Cameron A. G. W., Press W. H., Bowers R. L., 1990, ApJ, 348, 647

Bonnell I. A., Bate M. R., 2002, MNRAS, 336, 659

Bonnell I. A., Bate M. R., Clarke C. J., Pringle J. E., 1997, MNRAS, 285, 201

Bonnell I. A., Bate M. R., Clarke C. J., Pringle J. E., 2001, MNRAS, 323, 785

Bonnell I. A., Bate M. R., Vine S. G., 2003, MNRAS, 343, 413

Bonnell I. A., Larson R. B., Zinnecker H., 2007, in Reipurth B., Jewitt D., Keil K., eds, Protostars and Planets V. Univ. Arizona Press, Tucson, p. 149

Bontemps S. et al., 2001, A&A, 372, 173

Boss A. P., Fisher R. T., Klein R. I., McKee C. F., 2000, ApJ, 528, 325

Bouy H., Brandner W., Martín E. L., Delfosse X., Allard F., Basri G., 2003, AJ, 126, 1526

Bouy H., Martín E. L., Brandner W., Zapatero-Osorio M. R., Béjar V. J. S., Schirmer M., Huélamo N., Ghez A. M., 2006, A&A, 451, 177

Boyd D. F. A., Whitworth A. P., 2005, A&A, 430, 1059

Burgasser A. J., Reid I. N., Siegler N., Close L., Allen P., Lowrance P., Gizis J., 2007, in Reipurth B., Jewitt D., Keil K., eds, Protostars and Planets V. Univ. Arizona Press, Tucson, p. 427

Chabrier G., 2003, PASP, 115, 763

Close L. M., Siegler N., Freed M., Biller B., 2003, ApJ, 587, 407

Close L. M. et al., 2007, ApJ, 660, 1492

Davis C. J., Mundt R., Eisloeffel J., 1994, ApJ, 437, L55

Davis C. J., Eisloeffel J., Ray T. P., Jenness T., 1997, A&A, 324, 1013

Delgado-Donate E. J., Clarke C. J., Bate M. R., 2004, MNRAS, 347, 759

Delgado-Donate E. J., Clarke C. J., Bate M. R., Hodgkin S. T., 2004, MNRAS, 351, 617

Duchêne G., Bouvier J., Simon T., 1999, A&A, 343, 831

Duchêne G., Bontemps S., Bouvier J., André P., Djupvik A. A., Ghez A. M., 2007, A&A, 476, 229

Duquennoy A., Mayor M., 1991, A&A, 248, 485

Eisloffel J., Smith M. D., Davis C. J., Ray T. P., 1996, AJ, 112, 2086

Fekel F. C. Jr, 1981, ApJ, 246, 879

Fischer D. A., Marcy G. W., 1992, ApJ, 396, 178

Ghez A. M., Neugebauer G., Matthews K., 1993, AJ, 106, 2005

Gizis J. E., Reid I. N., Knapp G. R., Liebert J., Kirkpatrick J. D., Koerner D. W., Burgasser A. J., 2003, AJ, 125, 3302

Goodwin S. P., Whitworth A. P., Ward-Thompson D., 2004a, A&A, 419, 543

Goodwin S. P., Whitworth A. P., Ward-Thompson D., 2004b, A&A, 414, 633

Goodwin S. P., Whitworth A. P., Ward-Thompson D., 2004c, A&A, 423, 169

Goodwin S. P., Whitworth A. P., Ward-Thompson D., 2006, A&A, 452, 487

Greissl J., Meyer M. R., Wilking B. A., Fanetti T., Schneider G., Greene T. P., Young E., 2007, AJ, 133, 1321

Grether D., Lineweaver C. H., 2006, ApJ, 640, 1051

Guthrie B. N. G., 1985, MNRAS, 215, 545

Halbwachs J. L., Mayor M., Udry S., Arenou F., 2003, A&A, 397, 159

Hale A., 1994, AJ, 107, 306

Hall S. M., Clarke C. J., Pringle J. E., 1996, MNRAS, 278, 303

Hennebelle P., Fromang S., 2008, A&A, 477, 9

Hennebelle P., Teyssier R., 2008, A&A, 477, 25

Hillenbrand L. A., Hartmann L. W., 1998, ApJ, 492, 540

Hubber D. A., Whitworth A. P., 2005, A&A, 437, 113

Hubber D. A., Goodwin S. P., Whitworth A. P., 2006, A&A, 450, 881

Jensen E. L. N., Mathieu R. D., Donar A. X., Dullighan A., 2004, ApJ, 600, 789

Joergens V., 2006, A&A, 448, 655

Klessen R. S., 2001, ApJ, 556, 837

Klessen R. S., Burkert A., 2000, ApJS, 128, 287

Klessen R. S., Burkert A., 2001, ApJ, 549, 386

Klessen R. S., Burkert A., Bate M. R., 1998, ApJ, 501, L205

Köhler R., Petr-Gotzens M. G., McCaughrean M. J., Bouvier J., Duchêne G., Quirrenbach A., Zinnecker H., 2006, A&A, 458, 461

Konopacky Q. M., Ghez A. M., Rice E. L., Duchêne G., 2007, ApJ, 663, 394

Koresko C. D., 1998, ApJ, 507, L145

Kouwenhoven M. B. N., Brown A. G. A., Kaper L., 2007, A&A, 464, 581

Kratter K. M., Matzner C. D., 2006, MNRAS, 373, 1563

Kraus A. L., White R. J., Hillenbrand L. A., 2005, ApJ, 633, 452

Kraus A. L., White R. J., Hillenbrand L. A., 2006, ApJ, 649, 306

Kroupa P., 2001, MNRAS, 322, 231

Krumholz M. R., 2006, ApJ, 641, L45

Larson R. B., 1969, MNRAS, 145, 271

Larson R. B., 1981, MNRAS, 194, 809

Law N. M., Hodgkin S. T., Mackay C. D., 2008, MNRAS, 384, 150

Leinert C., Zinnecker H., Weitzel N., Christou J., Ridgway S. T., Jameson R., Haas M., Lenzen R., 1993, A&A, 278, 129

Li P. S., Norman M. L., Mac Low M.-M., Heitsch F., 2004, ApJ, 605, 800

Low C., Lynden-Bell D., 1976, MNRAS, 176, 367

Luhman K. L., 2004, ApJ, 614, 398

Luhman K. L., 2007, ApJS, 173, 104

McCarthy C., Zuckerman B., 2004, AJ, 127, 2871

McDonald J. M., Clarke C. J., 1993, MNRAS, 262, 800

McDonald J. M., Clarke C. J., 1995, MNRAS, 275, 671

Marcy G. W., Butler R. P., 2000, PASP, 112, 137

Martín E. L. et al., 2000, ApJ, 543, 299

Martín E. L., Barrado y Navascués D., Baraffe I., Bouy H., Dahm S., 2003, ApJ, 594, 525

Mason B. D., Gies D. R., Hartkopf W. I., Bagnuolo Jr. W. G., ten Brummelaar T., McAlister H. A., 1998, AJ, 115, 821

Masunaga H., Inutsuka S.-I., 2000, ApJ, 531, 350

Matzner C. D., Levin Y., 2005, ApJ, 628, 817

Maxted P. F. L., Jeffries R. D., 2005, MNRAS, 362, L45

Maxted P. F. L., Jeffries R. D., Oliveira J. M., Naylor T., Jackson R. J., 2008, MNRAS, 385, 2210

Mazeh T., Simon M., Prato L., Markus B., Zucker S., 2003, ApJ, 599, 1344

Monaghan J. J., 1992, ARA&A, 30, 543

Monaghan J. J., Gingold R. A., 1983, J. Comp. Phys., 52, 374

Monin J.-L., Menard F., Duchene G., 1998, A&A, 339, 113

Monin J.-L., Ménard F., Peretto N., 2006, A&A, 446, 201

Offner S. S. R., Klein R. I., McKee C. F., 2008, ApJ, 686, 1174

Ostriker E. C., Stone J. M., Gammie C. F., 2001, ApJ, 546, 980

Patience J., Ghez A. M., Reid I. N., Matthews K., 2002, AJ, 123, 1570

Pinfield D. J., Dobbie P. D., Jameson R. F., Steele I. A., Jones H. R. A., Katsiyannis A. C., 2003, MNRAS, 342, 1241

Preibisch T., Balega Y., Hofmann K.-H., Weigelt G., Zinnecker H., 1999, New Astron., 4, 531

Price D. J., Bate M. R., 2007, MNRAS, 377, 77

Price D. J., Bate M. R., 2008, MNRAS, 385, 1820

Rafikov R. R., 2005, ApJ, 621, L69

Rees M. J., 1976, MNRAS, 176, 483

Reid I. N., Lewitus E., Allen P. R., Cruz K. L., Burgasser A. J., 2006, AJ, 132, 891

Reid I. N., Cruz K. L., Burgasser A. J., Liu M. C., 2008, AJ, 135, 580

Reipurth B., Clarke C., 2001, AJ, 122, 432

Salpeter E. E., 1955, ApJ, 121, 161

Scally A., Clarke C., 2002, MNRAS, 334, 156

Siegler N., Close L. M., Mamajek E. E., Freed M., 2003, ApJ, 598, 1265

Siegler N., Close L. M., Cruz K. L., Martín E. L., Reid I. N., 2005, ApJ, 621, 1023

Silk J., 1977a, ApJ, 214, 152

Silk J., 1977b, ApJ, 214, 718

Simon M. et al., 1995, ApJ, 443, 625

Soderhjelm S., 1997, in Docobo J. A., Elipe A., McAlister H., eds, Astrophys. Space Sci. Library Vol. 223, Visual Double Stars: Formation, Dynamics and Evolutionary Tracks Astrophysics and Space Science Library, p. 497

Söderhjelm S., 2007, A&A, 463, 683

Stapelfeldt K. R., Krist J. E., Menard F., Bouvier J., Padgett D. L., Burrows C. J., 1998, ApJ, 502, L65

Sterzik M. F., Durisen R. H., 1998, A&A, 339, 95

Sterzik M. F., Durisen R. H., 2003, A&A, 400, 1031

Sterzik M. F., Tokovinin A. A., 2002, A&A, 384, 1030

Tokovinin A. A., 1993, Astron. Lett., 19, 383

Tokovinin A. A., 2000b, A&A, 360, 997

Tokovinin A., 2008, MNRAS, 389, 925

Tokovinin A., 2000a, in Zinnecker H., Mathieu R., eds, Proc. IAU Symp. 200, Birth and Evolution of Binary Stars, Astron. Soc. Pac., San Francisco, p. 84

Truelove J. K., Klein R. I., McKee C. F., Holliman J. H. II, Howell L. H., Greenough J. A., 1997, ApJ, 489, L179

van Albada T. S., 1968, Bull. Astron. Inst. Neth., 20, 73

Weis E. W., 1974, ApJ, 190, 331

Whitehouse S. C., Bate M. R., 2006, MNRAS, 367, 32

Whitworth A. P., 1998, MNRAS, 296, 442

Whitworth A. P., Stamatellos D., 2006, A&A, 458, 817

Wolf S., Stecklum B., Henning T., 2001, in Zinnecker H., Mathieu R., eds, Proc. IAU Symp. 200, Birth and Evolution of Binary Stars. Astron. Soc. Pac., San Francisco, p. 295

Worley C. E., 1967, Commun. Obs. R. Belgique Ser. B, 17, 221

This paper has been typeset from a TEX/LATEX file prepared by the author.